(Received 18 July 2025, Accepted 24 November 2025, Scheduled 15 December 2025)

Radio-Frequency Subwavelength Time-Reversal Imaging and Focusing: A Review of Theory, Methods, and Applications

Elias Le Boudec[1,*], Hamidreza Karami[3], Farhad Rachidi[1], Marcos Rubinstein[3], and Felix Vega[2]

[1] *Electromagnetic Compatibility Laboratory EPFL (The Swiss Federal Institute of Technology in Lausanne), Lausanne 1015, Switzerland*
[2] *Directed Energy Research Center, Technology Innovation Institute, Abu Dhabi, United Arab Emirates*
[3] *Institute for Information and Communication Technologies University of Applied Sciences and Arts Western Switzerland, Yverdon-les-Bains 1401, Switzerland*

ABSTRACT: Time reversal is an established wave imaging and focusing method that has proved to be robust and compatible with super-resolution imaging and focusing, i.e., to provide images and foci with subwavelength features beyond the diffraction limit. The method has been applied to numerous wave systems. We propose a systematic review of super-resolution time reversal applied to electromagnetic waves in the radio-frequency regime. We examine the theoretical foundation, the methods and the applications of radio-frequency super-resolution time-reversal. We explain a seeming contradiction between a widely used model of resolution due to the time-reversal cavity, and a common approach of Fourier optics highlighting the significance of evanescent waves for super-resolution. We also present an application of one of the algorithms of time-reversal imaging (known as TR-MUSIC) to measurements in a highly reflective environment, such as a resonant cavity. Finally, we outline open questions and applications.

1. INTRODUCTION

One of the most remarkable features of many wave systems is that their behaviour is largely unaffected by the direction of time. Given a wave $f(t, \mathbf{r})$, its time-reversed counterpart $f(-t, \mathbf{r})$ is — usually — physical and, more importantly, can be realised in practice using limited measurements of $f(t, \mathbf{r})$. Concretely, the emitted wave is measured on one or several sensors, the measurement is time-reversed, and sent back from these sensors. This process gave rise to the name "time-reversal mirror" (TRM) for such sensors. It can be used to focus waves and to image their source. In this case, in the "direct-time" stage, the fields emitted are recorded on the time-reversal mirror. In the "backpropagation" stage, the time-reversed waveforms are propagated back from the mirror into the medium. This stage is often performed in a digital full-wave equivalent of the system.

Unfortunately, time reversal is marred by the same limitation as classical optical lenses: the diffraction limit, i.e., the fact that two point sources placed less than $\sim\lambda/2$ apart, where λ is the wavelength, appear as a single point source. In radio frequencies, this means that features as large as hundred millimetres at gigahertz frequencies are blurred, hindering practical applications such as medical imaging. As a consequence, there has been significant effort to overcome this resolution limit, resulting in so-called "super-resolution" techniques. The pervasiveness of radio-frequency wireless systems and techniques (low-cost medical and scientific imaging, radars, high-throughput or low-power embedded or wearable communication devices, wireless power transfer, to name a few) has increased the need for these super-resolution techniques. The goal of this review is to highlight and summarize the development in theory, methods, and applications of these techniques, while also proposing areas of investigations that are yet to be developed.

To the best of our knowledge, no review has yet systematically addressed the proposed scope (time reversal, radio frequencies, and super-resolution). Indeed, the focus is either on the optical regime [1–3] or on specific techniques such as metamaterials [4–6], non-destructive testing [7], geophysical and biological media [8], power networks [9], or they share part of a common scope but are now outdated [10, 11]. There is a large intersection between the time-reversal method and the broader field of far-field subwavelength imaging (FFSI), which we do not discuss in details here. FFSI includes numerous applications and methods such as point spread function modulation [12], subwavelength MRI (magnetic resonance imaging) enhanced by planar and bulk metamaterials [13–15], image reconstruction from multiple MRI scans [16], and the so-called SREMI method for ground-penetrating radar [17], among others. We refer to the review by Astratov et al. [18] for a discussion of some aspects of the time-reversal method within FFSI.

The systematic process used to find relevant references is detailed in Appendix A. The review is structured as follows: We begin with various theoretical tools and analyses in Section 2, then review common methods for super-resolution imaging and focusing in Section 3 and their applications in Section 4. Finally, we conclude with a summary, remarks on methodological issues and an outlook in Section 5. Moreover, we explain the seeming contradiction in resolution between the time-

* Corresponding author: Elias Le Boudec (elias.leboudec@alumni.epfl.ch).

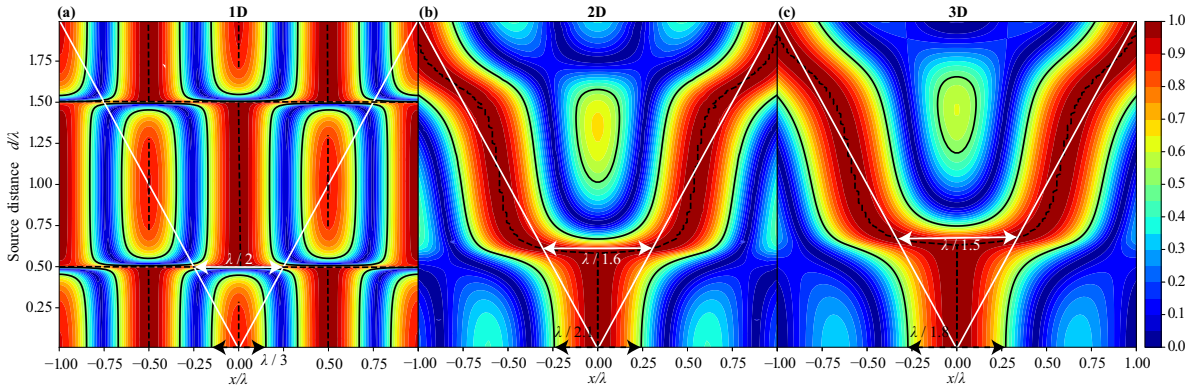

FIGURE 1. x slice at $y = 0$ from the (a) 1D, (b) 2D, and (c) 3D point-spread functions of two coherent in-phase sources separated by a distance d. For each separation, the x slice is max-normalised. The positions of the two sources are indicated by the white lines. Solid black: half-max isolines. Dashed black: maximum along x.

reversal cavity and Fourier optics. We also report our own application of the so-called TR-MUSIC algorithm to a resonant cavity.

2. THEORETICAL CONTRIBUTIONS TO SUBWAVELENGTH TIME-REVERSAL IMAGING AND FOCUSING

This section reviews theoretical contributions to subwavelength time-reversal imaging and focusing.

2.1. Super-Resolution Metrics

We start with an aside on the diffraction-limited resolution attainable by the time-reversal method in the electromagnetic regime and ways to measure it. Note that we base our analysis on the theory of the time-reversal cavity (see [19] or Section 2.3 below) and not the classical Rayleigh-Abbe diffraction limit. Quantitative analyses of super-resolution rely on metrics that evaluate the achieved focusing or imaging resolution. There are two commonly used metrics: (i) the full width at half-maximum (FWHM), which measures the width at half peak value of the point spread function (i.e., the image or focusing of a point source), and (ii) the capability of the system to distinguish two closely spaced sources. Note that most of the time, the full width at half-maximum is given for a linear quantity (voltage, electric field), and not the power. While it is reasonable to use the power, the obtained metric seems to perform better than with a linear quantity, as the power is a quadratic function of the field or voltage (and the same for higher orders [20]).

To give a baseline and contrast the two metrics (the full width at half-maximum and the distinction of neighbouring sources), we propose the following analysis. We consider the point-spread function of two neighbouring, in-phase, z-polarised dipoles (at $x = \pm d/2$ and $y = z = 0$) separated by a distance d in a vacuum as predicted by the time-reversal cavity [19]. This function describes the image that would be obtained by performing time reversal on a perfect time-reversal mirror (one that entirely surrounds the sources). We illustrate the x slice at $y = 0$ from this point-spread function (norm of the electric field) in Figure 1 for varying source separations. Both metrics can be readily derived from this plot. First, for a source separation $d = 0$, we get the point-spread function of a single source and we can derive a full width at half-maximum of $\lambda/1.8$, where λ is the wavelength of illumination. Second, by observing the smallest non-zero source separation at which the image maxima match with the source position, we see from Figure 1 that a separation of two neighbouring sources of more than $\lambda/1.5$ is necessary to distinguish them. Note that these metrics differ slightly. For completeness, we repeat this experiment for the two- (resp. one-) dimensional case obtained by numerically integrating the three-dimensional Green's function over the entire z (resp. y and z) axis. The results are presented in Table 1. These numbers show that, while the diffraction limit is usually described by $\lambda/2$, the actual limit of the system might range from $\lambda/3$ to $\lambda/1.6$.

TABLE 1. Metrics obtained from Green's functions.

Dimensionality	Full width at half-maximum	Min. source separation
1D	$\lambda/3$	$\lambda/2$
2D	$\lambda/2.1$	$\lambda/1.6$
3D	$\lambda/1.8$	$\lambda/1.5$

In some cases, the resolution is not the most relevant metric: for instance, in medical imaging (see Section 4.2) for the detection of tumours (which present a low contrast compared to neighbouring media), the signal-to-clutter ratio is preferred. In the presence of noise or back-propagation mismatch, the localisation error might also be more appropriate. Ghaderi Aram et al. also investigate time-reversal under a correlation index for total image quality [21].

2.2. Multiple Scattering and Random Media

Part of the allure of time reversal is its "self focusing" capability in complex media: no matter their complexity, time reversal ensures the focusing of waves in space and time. These complex media are typically categorised as either multiple scattering media (i.e., highly inhomogeneous media) or random media. While the latter category shares physical propagation char-

acteristics with the former, its random nature necessitates different analyses.

2.2.1. Multiple Scattering Media

Bal and Ryzhik [22] showed that, in the acoustic regime, "contrary to intuition, multiple scattering enhances the spatial resolution of the refocused signal and allows one to beat the diffraction limit obtained in homogeneous media." They provide quantitative predictions on the attainable resolution based on a convolution of the source with a medium-dependent filter.

Later, Fink summarised the important link between time reversal, multiple scattering and super-resolution [23]. While an ideal time-reversal mirror samples continuously over a closed surface (see Section 2.3), practical time-reversal mirrors are discrete and cover only limited angular apertures, leading to degraded focusing in homogeneous media. Yet, when multiple scattering or reflections occur, even a small-aperture mirror can exploit the medium's complexity to sharpen focus. This can be explained by the "kaleidoscopic" effect seen in environments with reflective boundaries, such as waveguides. Fink shows that in a parallel-walled acoustic waveguide, multiple reflections create virtual images of the time-reversal mirror. Recording over a sufficiently long time window captures these multipath arrivals, effectively expanding the aperture by the number of echoes and improving lateral resolution by up to an order of magnitude compared to free-space focusing.

Later, Shi and Nehorai [24] quantitatively confirmed this resolution improvement in scattering media by comparing the Cramér-Rao bounds with and without multiple scattering. Ammari et al. [25] further developed a mathematical framework to predict super-resolution in high-contrast media. Finally, multiple scattering can also provide super-resolution through a different mechanism: Simonetti [26] showed that multiple scattering within inhomogeneous media enables super-resolution by allowing the propagation of evanescent waves from the source to a far-field time-reversal mirror. In this case, the resolution-enhancement mechanism is not through the improvement of antenna aperture, but by recording of evanescent waves.

2.2.2. Random Media

Random media are complex materials in which the precise spatial distribution of inhomogeneities is unknown, but certain statistical characteristics are known. An example is the propagation of electromagnetic waves through Earth's atmosphere [27]. Fouque and Solna [28] show that, in the acoustic regime, as for multiple scattering media, the randomness improves the focusing resolution. Again, super-resolution is caused by an increase of the time-reversal mirror effective aperture. This property has been numerically verified [29] for random inclusions [30], continuous random media and varying polarisation [31], and random waveguides [32]. Moreover, the time-reversal process is statistically stable (or self-averaging) [33], meaning that the backpropagation focusing occurs near the source irrespective of random realisations. Ishimaru et al. [27] provide a comparison of several imaging methods, including classical time reversal and time-reversal MUSIC (see Section 3.3.2) in random media.

2.3. The Time-Reversal Cavity

We have seen that the imaging or focusing resolution of a time-reversal system depends on the effective aperture of the time-reversal mirror. However, previous analyses in the optical regime (discussed in Section 3.3.2 below) also show that the diffraction limit arises from the inability of waves with wavenumbers larger than the free-space wavenumber $k_0 = 2\pi f/c_0$ (where c_0 is the free-space speed of light and f is the frequency) to propagate. Such waves are called "evanescent" as they decay exponentially away from sources or scatterers. The time-reversal cavity, described by Carminati et al. [19], offers a theoretical framework to describe the resolution attainable in an inhomogeneous, possibly anisotropic, medium. By using Green's (or the divergence) formula, the time-reversal mirror becomes a closed surface where the time-reversed field is integrated to obtain the diffraction-limited field inside the cavity. Carminati et al. show that the focal spot (or point-spread function) at a single frequency is given by the imaginary part of Green's function. For a scalar wave in a vacuum, this imaginary part behaves like a sinc function, and we obtain the diffraction limit illustrated in Figure 1. To obtain a super-resolution system, one must design structures where the imaginary part of Green's function oscillates on a subwavelength scale. Of course, the theory is not as descriptive for broadband excitations, as an inverse Fourier transform is needed for time-domain excitations. Le Boudec et al. extended this theory for nonreciprocal media [34] and provided a heuristic to determine the point-spread function from the medium's dispersion relation.

2.4. The Time-Reversal Mirror

In its theoretical form, the time-reversal mirror (TRM) is an idealised, continuous sensing, and closed surface surrounding the region of interest (which either contains the source to be imaged or the target location for wave focusing). We have seen that in practice, the finite aperture of a time-reversal mirror results in a reduced resolution, a limitation that can be mitigated by the presence of a multiple scattering or random medium. Moreover, we discuss in Section 3.2.2 that the distance between an ideal time-reversal mirror and the source does not matter for super-resolution focusing. In fact, this was already noted by de Rosny and Fink [35]. From the divergence theorem, they decompose the ideal time-reversal mirror [19] into monopole and dipole mirrors. The monopole time-reversal mirror stems from Green's function G, and the dipole from its normal derivative $\partial G/\partial \mathbf{n}$. While the ideal time-reversal is diffraction-limited, the monopole-only and dipole-only mirrors can "record" evanescent waves. Thanks to its directivity, the dipole-only mirror can moreover improve the resolution beyond the diffraction limit when placed in the source near-field. This research has then been extended to multiple scattering media [36]. An original approach consists in an optimised adjustment of the weights of time-reversal mirror channels to maximize the resolution [37]. However, some prior information about the imaged system is needed.

Related work by Farhi [38] introduces a different view of the time-reversal mirror. He proposes to tailor the resonance of a dielectric spherical shell to possess a resonance for a given

multipole field. This finds applications when the realisation of a time-reversal mirror using discrete sensors is impossible. By exciting the shell with a dipole placed at an arbitrary location outside of it, a given multipole field can be excited inside the shell, possibly with super-resolution focus.

2.5. Transmission Line Networks

The transient analysis of networks of power lines is an interesting tool to locate faults (e.g., short circuits). Branches of these networks can be modelled as transmission lines, and their single-dimensional nature makes it the first application of an experimental and ideal time-reversal cavity [39]. To the best of our knowledge, applications of time-reversal imaging or focusing in two-dimensional transmission line networks (for example, a fully meshed network) have not been reported. The resolution obtained in an experimental case study by Wang et al. [40] is remarkably high. For a solid phase (a)-to-ground fault (i.e., a short circuit between phase (a) and ground), an equivalent[1] full width at half-maximum of roughly 1'100 m is obtained. The fault voltage features oscillations at ∼5 kHz, which entails a resolution around $\lambda/55$.

In fact, He et al. provide a theoretical analysis [41] of the obtained resolution in transmission line networks. They derive the distribution of the correlation between the measured signal and those obtained at probe locations,

$$\rho(x) \propto \int \mathrm{d}\omega |V_f(\omega)|^2 H^*(\omega, 0) H(\omega, x) \qquad (1)$$

where x is the probe location; V_f is the surge signal; and $H(\omega, x)$ is the response of a line to a source placed at the location x. It is assumed that the actual source is placed at the origin. While this does not correspond to traditional time-reversal, there is a strong link because of the time-reversal operator H^*H. The results from a single-phase lossless overhead line, with an example in Figure 2, show super-resolution around $\lambda/67$. This behaviour is caused by the resonances in lines with high-impedance terminations, such as transformers, and it is influenced by propagation losses. Finally, contrary to intuition, extending the analysis from a single line to a network with lateral branches or to three-phase systems decreases the resolution [41]. In this reference, the deterioration is treated as a reduction of the system sensitivity to the fault position, and is not associated with higher losses linked to an overall longer transmission line. This seems to oppose the earlier notion that multiple scattering increases resolution through a larger effective aperture, warranting further investigation to understand the underlying physical limitation and to allow a reliable application of the method in power networks.

2.6. The Instantaneous Time-Reversal Mirror

Because of the usual duality between space and time in wave physics, we expect a dual of the time-reversal mirror to exist.

[1] The considered fault in [40, Figure 17] occurs close to a line end (node 55); the full width at half-maximum can only be determined in one direction, at node 49, which is 312 m + 230 m away from the fault. We double this distance by symmetry — which, of course, is a simplification — to obtain 1'084 m.

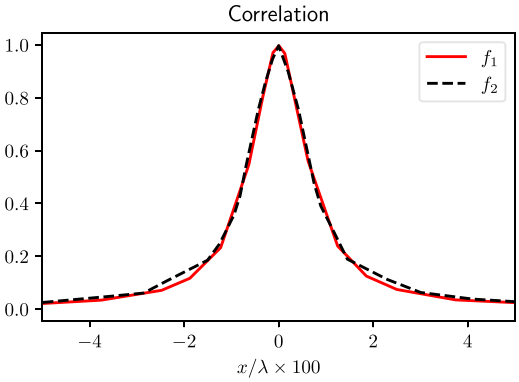

FIGURE 2. Correlation functions $\rho(x)$ for the transfer functions in a line with a fault 6 km from the probe for two resonances, $f_1 = 37.3$ kHz and $f_2 = 87.6$ kHz at the fault location. The x axis is normalised with respect to the corresponding wavelength. Adapted from the data in [41].

The time-reversal mirror reverses measurements over time on a spatial boundary, i.e., a surface, whose dimensionality is one less than the dimensionality of spatial propagation. The dual object should reverse measurements over the entire space on a temporal boundary. Since we expect time to flow only in one dimension, this boundary has to be an instant, i.e., a point in time. Indeed, this corresponds to the concept of instantaneous time-reversal mirror [11]: an instantaneous discontinuity in the entire space (e.g., a Dirac spike in the propagation speed) creates a time-reversed wavefront that converges back to the original source. This is interesting as no recording of the wave by sensors is needed. Moreover, this process benefits from the same resolution enhancement in multiple scattering media [42] as the classical time-reversal mirror.

2.7. Negative Transient-Flux

The significance of evanescent waves to super-resolution motivates a careful analysis of small (subwavelength) sources, such as point sources. Bossy and Carminati [43] analyse the near-field of a transient point source and show that some energy is re-absorbed by the source before being emitted as radiation. This has been experimentally confirmed [44]. Of particular interest to us, a consequence of this transient absorption of the source is that "perfect subwavelength refocusing (i.e., without energy scattered away from the focal spot) cannot be achieved by use of a passive subwavelength absorber [...] since the dynamic exchange of energy is a necessary condition for a localised absorption of the full energy of the wave field" [43]. This statement is directly linked to the concept of the time-reversal sink, discussed in Section 3.1 below. Indeed, this suggests that the highest resolution can only be attained by active sinks, i.e., those that can partially and momentarily re-emit the absorbed energy.

This fact resonates with the standard analysis of reactive energy, a classical concept of electrical engineering. The concept could be linked to the reactive power in an inductor or capacitor, which is really stored as potential energy of a field (magnetic for the inductor, electric for the capacitor). There is no radiation because the size of such devices is small compared to the wavelength.

3. METHODS FOR SUBWAVELENGTH TIME-REVERSAL IMAGING AND FOCUSING

In this section, we cover practical methods used in conjunction with time reversal that have been shown to achieve super-resolution focusing or imaging.

3.1. The Time-Reversal Sink

The theory of the time-reversal cavity demonstrates that the diffraction limit in time-reversal imaging or focusing can be explained by the interference between the converging and diverging wavefronts [19] (see Section 3.2.2). In fact, this can also be seen by the mismatch between the direct-time field, which is emitted by a source, and the time-reversed field, which lacks a corresponding time-reversed source. As a result, the energy of the time-reversed field cannot be absorbed by the original source and must continue to propagate.

This consideration brings up the idea of a time-reversed "sink", whose role is to absorb the energy of the converging time-reversed wave. De Rosny and Fink showed that an experimental realisation of such a sink is not only possible, but also yields super-resolution [45]. This sink can also be connected to the generation of the evanescent waves, which are necessary for achieving super-resolution imaging or focusing. In the cited work, the same acoustic transducer is used both as the direct-time source and the time-reversal sink, an ideal case scenario. In fact, the resolution appears to be limited only by the physical size of the transducer.[2]

A weaker version of the time-reversal sink involves placing passive absorbers at the original source location [47]. Such an approach also leads to super-resolution. Ma et al. [47] achieve super-resolution with a purely passive component (an absorber). However, the existence of the negative transient flux presented in Section 2.7 suggests that a perfect time-reversal sink needs to be able to perform both absorption and emission. This prompts the apparently still open question: Is there a fundamental physical limit to the extent to which passive absorbers can act as time-reversal sinks, or does the discrepancy reflect a subtle difference in interpretation between the two approaches?

3.2. Metamaterials

Metamaterials are synthetic materials whose subwavelength structure is designed to possess a given macroscopic behaviour unavailable in natural materials.

3.2.1. Lenses

Our first class of metamaterials is of particular historical significance. Lenses are designed to focus waves in a given region to allow imaging by direct sampling of the field. The promise of super-resolution is rooted in the idea of a "perfect lens" [48], also linked to time reversal by Pendry [49]. Liao et al. realise a limited version of such a lens (based on enhancement of evanescent waves) using a slab of multilayered dielectrics [50]; Katko et al. [51] use split-ring resonators loaded with varactor diodes to realize a phase-conjugation slab. Time-reversal is also used to design flat lenses [52].

3.2.2. Reconciling Super-Resolution Imaging Predictions from the Time-reversal Cavity and Fourier Optics

In Fourier optics [53], the diffraction limit is understood to arise from the evanescent nature of waves with high transverse numbers associated with fine (below the wavelength) source details.[3] In time reversal imaging, this same limit emerges from the interaction between the converging wave caused by the time-reversal mirror, and the diverging one that exists because of the absence of a time-reversal sink [19]. The latter limit exists irrespective of the shape of the time-reversal mirror; in particular, no matter how far the sensors are from the source. This seems to contradict the well-known fact that the capture of evanescent waves is key to beating the diffraction limit [48].

In this section, we show how to resolve this seeming contradiction, which results from a simplistic interpretation of both theories. We illustrate the results in a numerical simulation of a two-dimensional resonant metalens. Doing so, we summarize key properties that a time-reversal subwavelength imaging system must possess.

First, we review the origin of the diffraction limit in time-reversal and classical optics, highlight the seeming contradiction, propose an explanation to reconcile both approaches, and introduce the simulation setting used to test the explanation. We begin by recalling the theory of the time-reversal cavity for electromagnetic fields, introduced in [19] and extended in [34]. In this setting, a source radiates electromagnetic fields (the direct-time fields) which are then recorded on a closed time-reversal cavity surrounding the source. These fields are then time-reversed and propagated back from the cavity boundary.

Since the source is not present during this backpropagation stage, the time-reversed fields are the sum of a converging and a diverging wave to satisfy the source-free wave equation. In the frequency domain, if the direct-time electric field at an angular frequency $\omega = 2\pi f$ and position $\mathbf{r}$ is denoted by $E_{\mathrm{DT}}(\omega, \mathbf{r})$, then the time-reversed electric field is [19, 34]

$$E_{\mathrm{TR}}(\omega, \mathbf{r}) = E^{*}_{\mathrm{DT}}(\omega, \mathbf{r}) - E_{\mathrm{DT}*}(\omega, \mathbf{r}) \tag{2}$$

where $\cdot^{*}$ denotes complex conjugation. $E^{*}_{\mathrm{DT}}(\omega, \mathbf{r})$ is a converging wave, equal to the time-reversal of the direct time wave. $E_{\mathrm{DT}*}(\omega, \mathbf{r})$ is the diverging wave that would be radiated by the time-reversed original source. For an electric dipole, the time-reversed field is proportional to the imaginary part of the electric Green's function, exhibiting a sinc-like behaviour at the dipole location. The width of this sinc is determined by the free-space wavenumber k_0, resulting in an approximate focal spot size of $\lambda_0/2$.

In Fourier optics [53], we analyse the fields radiated by a planar source distribution in the xy-plane. The wavenumbers associated with the corresponding Fourier transform are k_x and k_y, and the propagation away from the source occurs in the z direction, associated with the wavenumber k_z. Outside the source region, the propagation obeys a wave equation whose

[2] For completeness, we note the work of Zverev [46] who argues that de Rosny et al. did not interpret the results correctly.

[3] This section is adapted and updated from [54].

dispersion relation is a sphere in wavenumber space such that

$$k_x^2 + k_y^2 + k_z^2 = k_0^2 \tag{3}$$

Hence, the fields radiate away from the source according to the positive solution

$$k_z = \begin{cases} \sqrt{k_0^2 - k_x^2 - k_y^2}, & k_x^2 + k_y^2 \leq k_0^2 \\ j\sqrt{-k_0^2 + k_x^2 + k_y^2}, & k_x^2 + k_y^2 > k_0^2 \end{cases} \tag{4}$$

where $j^2 = -1$. The propagation involves the delay operator $e^{-jk_z z}$. Hence, small source details, described by high transverse wavenumbers whose norms exceed k_0, have a purely imaginary wavenumber, and the corresponding wave decays exponentially. In other words, details finer than λ_0 are associated with evanescent waves, and far-field sensors must be diffraction-limited. For example [55], the imaging of a rectangular $\ell \times \ell$ aperture in a shield illuminated by a plane wave is a focal spot of surface $\sim\lambda_0^2$ when imaging from the far field. However, at distances less than roughly $\ell/3$, the evanescent wave carries information about the aperture's true size, that is, ℓ^2.

It should be pointed out here that the subwavelength details associated with the source near-field are technically always transmitted to the far zone. However, they decay as $1/r^3$, where r is the distance to the source, and are thus overwhelmed by the radiating part (in $1/r$).

The seeming contradiction is that, on the one hand, a consequence of Equation (2) is that the distance between the time-reversal mirror and the source is predicted to have no effect on the focal spot size (i.e., the imaging resolution) and, on the other hand, the source near-field is necessary to obtain subwavelength images (Equation (4)). The nuance needed to solve this seeming contradiction is that the Fourier optics approach does not describe how to obtain the image (e.g., through time-reversal, a classical optical lens, a near-field scan, etc.). Indeed, in agreement with the time-reversal theory, time-reversal imaging is always limited to resolutions dictated by Equation (2); however, this limited resolution might exhibit a $\lambda/2$ focal spot much smaller than in a vacuum, as long as $\lambda < \lambda_0$. An academic example is radio-frequency imaging in pure water, with a real part of the electrical permittivity of 80 [56] yielding a $\lambda_0/2/\sqrt{80} \approx \lambda_0/18$ super-resolution. Additionally, the time-reversal cavity does not provide an explanation of how to improve the imaging resolution (other than the use of a time-reversal sink [45]). There, the classical optical theory comes into play: a path towards super-resolution involves transmitting near-field information to the time-reversal mirror.

In summary, the Fourier optics approach shows that subwavelength information is contained in the source near field. The near-field waves then need to couple to the imaging system, without regard for the distance between the time-reversal mirror and the source region[4].

To illustrate the explanation above, we perform a set of two-dimensional radio-frequency simulations. The geometry of the experiments is shown in Figure 3. In the direct-time phase, we measure the scattering parameters from two simultaneous, identical sources (ports 1 and 2) placed $30\%\lambda_0$ ($\lambda_0 = 1\,\text{m}$) apart (at the positions $x = \pm 15\,\text{cm}$, $y = 0$) to a nine-channel time-reversal mirror indexed from 10 to 18, i.e.,

$$z_{\text{DT}}(f_n) = S_{m,1}(f_n) + S_{m,2}(f_n) \tag{5}$$

$m = 10, \ldots, 18$, over a frequency range f_n from 200 MHz to 300 MHz, every half megahertz ($n = 1, \ldots, 201$).

In the time-reversal phase, we measure the scattering parameter from each element of the time-reversal mirror to a port (0, not shown in Figure 3), placed on the source plane at position x, and vary x from $-50\,\text{cm}$ to $+50\,\text{cm}$ in steps of 5 cm, thus obtaining $S_{0,m}(f_n, x)$. We time-reverse the direct-time measurement by taking the complex conjugate of $z_{\text{DT}}(f_n)$. We backpropagate this time-reversed measurement to the image plane ($z = 0$) by multiplying by the scattering parameter $S_{0,m}(f_n, x)$, obtaining the time-reversed field along the x coordinate:

$$z_{\text{TR}}(f_n, x) = \sum_{m=10}^{18} S_{0,m}(f_n, x) z_{\text{DT}}(f_n)^* \tag{6}$$

Finally, we average the frequency dependence out by taking the normalised energy

$$z_{\text{TR}}(x) = \left[\frac{\sum_{f_n} |z_{\text{TR}}(f_n, x)|^2}{\sum_{f_n, m} |S_{0,m}(f_n, x)|^2} \right]^{1/2} \tag{7}$$

The denominator serves as a normalisation with respect to the source-to-time-reversal-mirror coupling strength.

Next, we study six imaging cases, illustrated in Figure 3:

(a) Propagation in vacuum, with a far-field time-reversal mirror;

(b) As (a), with a near-field time-reversal mirror;

(c) We introduce a resonant metalens as in [56, 57] with 41 metallic rods of height $\lambda_0/2$ and a pitch of $\lambda_0/40$. First, we place this lens far, i.e., $\lambda_0/2$, from the source, with a far-field time-reversal mirror. The lens supports resonant eigenmodes that are transversally subwavelength, and whose far-field radiation pattern can be used to reconstruct a subwavelength image.

(d) Next, we bring the metalens close ($\lambda_0/20$) to the source.

(e) We bring the time-reversal mirror in the near-field from the source-and-metalens complex, with the metalens far ($\lambda_0/2$) from the source.

(f) Finally, we keep a near-field time-reversal mirror and bring the metalens close ($\lambda_0/20$) to the source.

The time-reversed energy $z_{\text{TR}}(x)$ is shown in Figure 4, along with an example of scattering parameter.

As the source separation is below the diffraction limit for a two-dimensional problem ($\lambda_0/1.7$ or $\sim 60\%\lambda_0$), the sources are indistinguishable without a resonant metalens. Including the metalens, both sources are clearly visible, as long as it is placed

[4] Of course, in practice, the time-reversal mirror is replaced with a finite number of sensors. The placement of these sensors is well known to be critical.

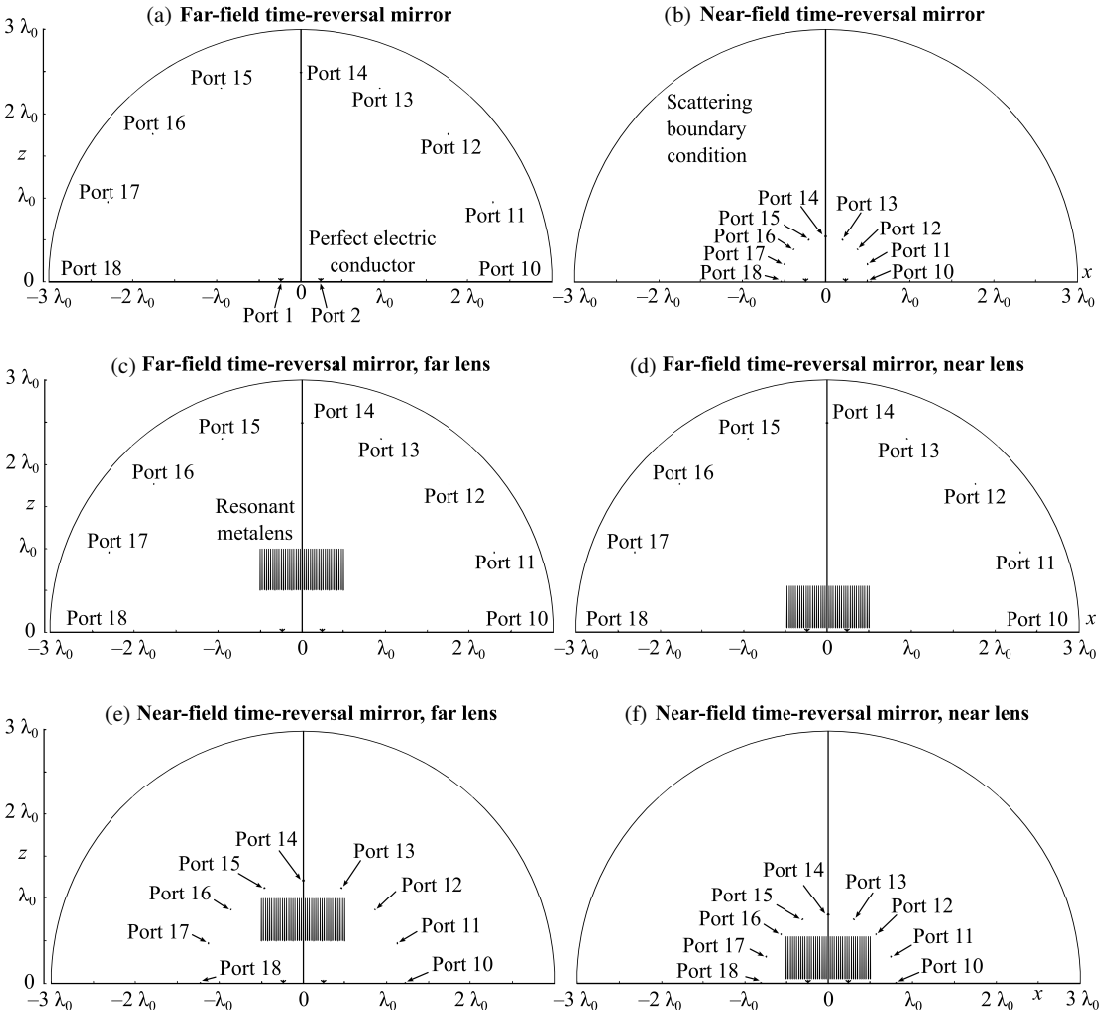

FIGURE 3. Geometries of all performed simulations. (a), (b) in a vacuum, with a (a) far-field and (b) near-field time-reversal mirror (TRM); (c), (d) with a resonant metalens placed (c) far or (d) near the sources, and a far-field time-reversal mirror; (e), (f) with a resonant metalens placed (e) far or (f) near the sources, and a near-field time-reversal mirror. The ports are simulated as electrically small lumped ports with a time-harmonic excitation.

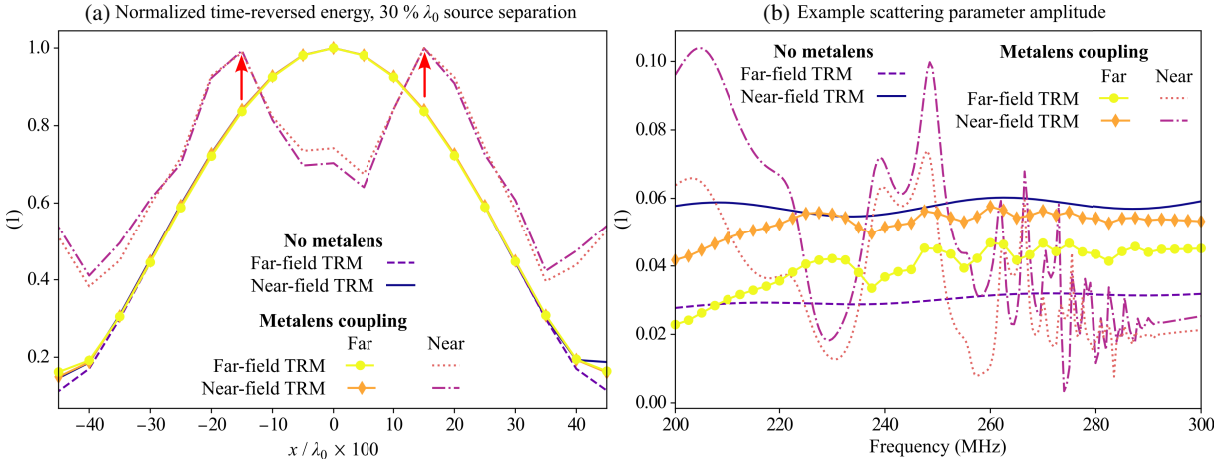

FIGURE 4. (a) Normalised time-reversed energy $z_{\mathrm{TR}}(x)$ as in Equation (7) for a source separation of $30\%\lambda_0$ and the cases shown in Figure 3. The original source positions are indicated by red arrows. (b) Example time-reversal scattering parameter $S_{0,10}(f_n, x = 0\,\mathrm{m})$ for all cases (a)–(f) in Figure 3.

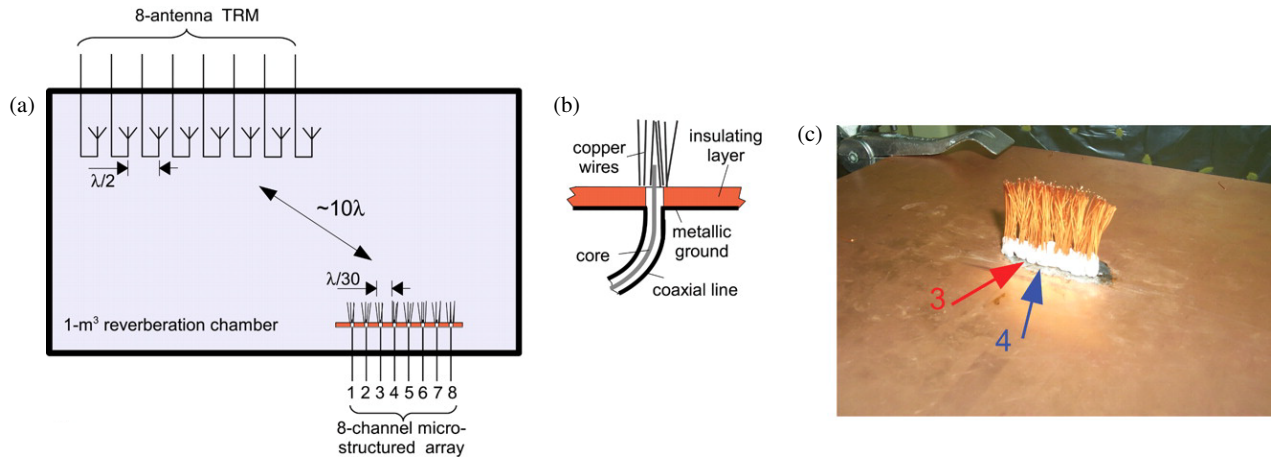

FIGURE 5. Microstructured antenna experiment in [70]. (a) A time-reversal mirror made of eight commercial dipole antennas operating at 2.45 GHz (i.e., $\lambda = 12$ cm) is placed in a 1 m^3 reverberating chamber. A subwavelength receiving array consisting of eight microstructured antennas $\lambda/30$ apart from one another is placed ten wavelengths away from the time-reversal mirror. (b) Details of one microstructured antenna. It consists of the core of a coaxial line that comes out 2 mm from an insulating layer and is surrounded by a microstructure consisting of a random distribution of thin copper wires. (c) Photo of the eight-element subwavelength array surrounded by the random distribution of copper wires. Antennas 3 and 4 are indicated by the red and blue arrows. Reproduced from Lerosey et al., Focusing Beyond the Diffraction Limit with Far-Field Time Reversal, Science, 10.1126/science.1134824 [2007], AAAS.

in the source near field. However, the placement of the time-reversal mirror, far or near the source, has no significant effect.

This reconciles both points of view, from the time-reversal cavity and Fourier optics: one the one hand, we need the evanescent waves for super-resolution, illustrated here by the necessity of i) capturing the evanescent components using the metalens in the source near-field, ii) and making these components visible to the time-reversal mirror by various resonances (see Section 3.2.3 or [59]); and, on the other, a near-field distance between the time-reversal mirror and the source is not, by itself, sufficient for super-resolution. In the conclusion, we discuss a more general statement about super-resolution requirements.

3.2.3. Other Metamaterials, Often Resonant

In 2010, Lemoult et al. [58] introduce a resonant metalens to provide far-field subwavelength imaging. This metamaterial consists of an array of metallic rods arranged on a subwavelength scale in the transverse xy plane. Individually, they possess a resonance at a frequency f_0 whose wavelength is double the rods' length. The array supports a wide number of eigenmodes whose wavenumbers exceed that of vacuum. In turn, a source with subwavelength feature can couple with those eigenmodes. Finally, each of these eigenmodes has a distinctive radiation pattern (dipole, x or y quadrupole, or octupole). See Lemoult et al. [59] for a detailed analysis of the resonant metalens. The time-reversal method enables to handle the complex mapping from subwavelength source to the far field. To note, this metalens' operation is inherently wideband: attempting to image a source at a bandwidth comparable to that of the eigenmodes will yield the periodic field distribution of that eigenmode. Beyond the point-spread function, the resonant metalens was used to image subwavelength details in [60], and in [61] with the time-reversal method. In this reference, the authors identified two main factors that limit resolution: the array pitch and the losses in the metalens. To maximize resolution, thin low-loss rods should be used with a narrow spacing.

Speaking of losses, Guan et al. [62] demonstrate the use of complex frequencies to compensate for losses in a hyperbolic metamaterial. These complex frequencies are designed to provide gain for wavenumbers which are of negligible amplitude, thereby enabling super-resolution. Importantly, this gain is applied virtually during postprocessing, without the need to physically realize active media.

Time-reversal imaging and focusing can also be applied to planar metamaterials, such as surfaces of split-ring resonators [63] (including an adaptation for magnetic sources [64]), fractal resonators [65] coupled with a resonant cavity for multi-incidence excitation, grating plates [66], spoof surface plasmon polaritons [67], or a recording metasurface with interpolation to compensate for low field sampling [68]. Wang et al. [69] propose using a metasurface with programmable defects which allows subwavelength imaging of intricate sources at the cost of requiring prior source knowledge.

Finally, de Rosny et al. [70] show the relevance of the impedance matrix for time-reversal focusing on antenna arrays.

3.2.4. A Widespread Approach: Microstructured Antennas

The term "microstructured antennas" [71] is used to describe metamaterial-based systems where antennas are placed in a subwavelength array and combined with near-field structures to enhance resolution. In a seminal work, Lerosey et al. [71] placed an eight-channel array of monopole antennas placed $\lambda/30$ apart. This array was then surrounded by randomly placed insulated copper wires (see Figure 5). Super-resolution at antenna array pitch scale is obtained by a similar mechanism to resonant metalenses: a subwavelength arrangement of scatter-

TABLE 2. Proposed microstructured antennas. *No experiment.

Ref.	Setup	Excitation band	Pitch
[71]	Random wires	2.45 GHz, bandwidth 150 MHz	4 mm
[72]	Planar antenna elements etched with defect oval rings	2.5–4.5 GHz	4.3 mm
[73]	Triangle monopole antennas etched with cross slots	2.5–4.5 GHz	4.3 mm
[74]	Planar monopoles etched with circular slots	Pulse centred at 4.5 GHz	3.3 mm
[75]	Array with chirped delay line feeds	3–6 GHz	2 mm
[76]	Split-ring-based metamaterial sheets	2–6 GHz	5 mm
[77]	Antennas with micro-structured fractal slots and split ring resonators*	2.5–5 GHz	10 mm
[78]	Planar resonant lens with periodically distributed strip resonators	1–2 GHz	10 mm
[79]	Array with pulse-shaping circuit feeds	3.5–6.5 GHz	10 mm
[80]	Array with non-reciprocal chirped delay line feeds	3–6 GHz	6.7 mm
[81]	Compact multiport antenna	2.5 GHz sinus, 3 periods	3 mm
[82]	2D array of monopoles*	2–6 GHz	2.1 mm
[83]	Two wire antennas for multi-frequency operation	1–1.5 GHz and 1.5–2 GHz	5 mm
[84]	Subwavelength scatterers and auxiliary source*	0–2 GHz	N/A
[85]	MIMO antenna with complementary split-rings*	2.4–2.8 GHz	∼35 mm
[86]	Random wire array with bowtie antenna-based time-reversal mirror*	3 ns Gaussian pulse at 2.45 GHz then 5.2 GHz	10 mm
[87]	Planar array of spiral resonators*	0.8–1.8 GHz	9.1 mm
[88]	2D array of cylindrical dielectric rods	3 GHz Ricker wavelet [88]	20 mm

ers (supporting high-wavenumber modes) whose effect is perceptible in the far field. Other related approaches are summarised in Table 2.

Among the proposed microstructured antennas, one distinct variation involves the use of dispersion in the antenna feeds [75, 79, 80]. This approach relies on engineering different antenna responses such that their cross-correlation is minimal. Finally, an important limitation of the methods presented in this section is that imaging and focusing are, by design, restricted to discrete antenna channels rather than continuous images. While this makes the approach less general, it allows for relatively high performance and finds applications in radio communications (see Section 4.3).

3.3. Algorithms

In this section, we group together all methods that enhance resolution not by altering the physical propagation characteristics of the system, but through advanced postprocessing techniques. These methods generally exploit prior knowledge of the underlying physical processes behind the data.

3.3.1. DORT

Is it possible to use time reversal in a multistatic radar setting? Prada et al. show it is, by introducing DORT (decomposition of the time-reversal operator[5]) [90]. While DORT alone does not usually lead to super-resolution images, we introduce the method here because its formalism is used in TR-MUSIC and other super-resolution variants, such as TR-ESPRIT [91].

[5]French: "Décomposition de l'opérateur de retournement temporel."

Assuming an array of M transmit-receive transducers, we measure the inter-elements transfer functions $H_{ij}(\omega)$, $1 \leq i, j \leq M$, and build the transfer matrix (i.e., multistatic data matrix) $\mathbf{H}(\omega)$. We send a pulse $\mathbf{c}(\omega)$ on the transducers and obtain the response $\mathbf{H}(\omega)\mathbf{c}(\omega)$. By time-reversing this response (i.e., taking the complex-conjugate, denoted by $\cdot^*$) and retransmitting it back from the array, we obtain the new measured response[6] $\mathbf{H}(\omega)\mathbf{H}^*(\omega)\mathbf{c}^*(\omega)$. The total operation (up to conjugation) corresponds to the time-reversal operator $\mathbf{H}^*(\omega)\mathbf{H}(\omega)$. Prada et al. show that, for up to M well-resolved reflective targets, the eigenvalues of $\mathbf{H}^*(\omega)\mathbf{H}(\omega)$ are linked to each target's reflectivity. By transmitting the corresponding eigenvector from the array, the resulting field focuses on the right target. Moreover, by sorting the (real and positive) eigenvalues, the number of scatterers can be estimated by counting those with significant magnitude.

3.3.2. TR-MUSIC

To improve the resolution of the DORT method, Devaney proposed (in an unpublished work) to combine it with the multiple signal classification (MUSIC) method [92]. This method, described in [93, 94], is known as TR-MUSIC[7]. To apply the method, we perform a singular value decomposition of the transfer matrix:

$$\mathbf{H}(\omega) = \mathbf{U}(\omega)\mathbf{S}(\omega)\mathbf{V}^{\dagger}(\omega) \tag{8}$$

[6]The imaged and imaging systems are assumed to be reciprocal, hence $\mathbf{H}(\omega)$ is symmetrical.

[7]The difference between TR-MUSIC and MUSIC is mainly syntactic; MUSIC, as originally introduced, focuses on angle-of-arrival estimation, and TR-MUSIC on source imaging.

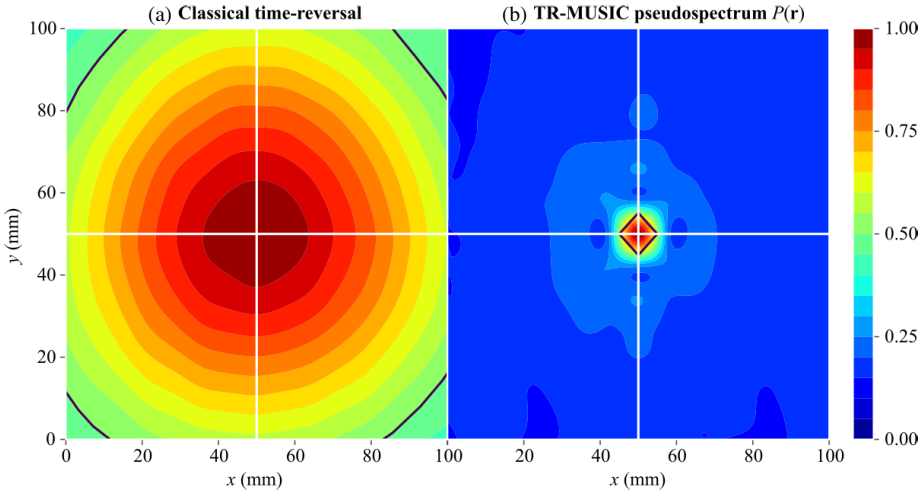

FIGURE 6. Point imaging in a resonant cavity. Max-normalised (a) point-spread function according to classical time-reversal and (b) pseudospectrum based on TR-MUSIC. The original source location $\mathbf{r}_0$ is indicated by the intersection of the white lines. The half-max isolines are shown in solid black.

using the unitary matrices $\mathbf{U}(\omega)$ and $\mathbf{V}(\omega)$. $\mathbf{S}(\omega)$ is a real diagonal matrix of singular values. We assume that the singular values have been sorted by decreasing order, so that the first column $\mathbf{u}_1(\omega)$ of $\mathbf{U}(\omega)$ corresponds to the largest singular value. $\cdot^\dagger$ denotes Hermitian conjugation. Note that the columns $\mathbf{u}_j(\omega)$, $j = 1, \ldots, M$ of $\mathbf{U}(\omega)$ (resp. $\mathbf{V}(\omega)$) correspond to eigenvectors of $\mathbf{H}(\omega)\mathbf{H}^\dagger(\omega)$ (resp. $\mathbf{H}^\dagger(\omega)\mathbf{H}(\omega)$), establishing the strong link with the DORT method. Unlike DORT, which assumes only the presence of a few well-resolved scattering sources as prior information, TR-MUSIC also incorporates a model of field propagation through "steering vectors" $\mathbf{a}(\omega, \mathbf{r})$ (a vector of length M) [92]. Often, it is sufficient to model propagation in vacuum,

$$\mathbf{a}(\omega, \mathbf{r}) \propto \left[e^{jk_0|\mathbf{r}-\mathbf{r}_i|}/|\mathbf{r}-\mathbf{r}_i|\right]_{i=1,\ldots,M} \tag{9}$$

where $\mathbf{r}_i$ are the transducer positions, and $k_0 = \omega/c_0$ is the free-space wavenumber where c_0 is the speed of light in vacuum. These steering vectors are introduced by computing the pseudospectrum

$$P(\omega, \mathbf{r}) = \frac{1}{\sigma_r + \sum_{j=N+1}^{M} |\mathbf{u}_j^\top(\omega)\mathbf{a}(\omega, \mathbf{r})|} \tag{10}$$

where σ_r is an optional regularisation parameter, and N is the expected number of scatterers. The rationale behind this formula is that the last $M-N$ left eigenvectors $\mathbf{u}_j(\omega)$ are assumed to correspond to noise; hence, when $\mathbf{r}$ matches the source location, $\mathbf{u}_j^\top(\omega)\mathbf{a}(\omega, \mathbf{r})$ is an eigenvalue corresponding to noise, hence, of negligible value. As a result, the pseudospectrum is maximised at the source location.

Subsequent work investigated the influence of noise [95] and polarisation [96], and introduced adaptations aimed at reducing computational resources [97], relaxing the frequency and array size requirements through time gating [98], enabling operation in highly cluttered environments [99], and achieving lower side-lobe levels and improved resolution in noisy data [100].

Illustration in a resonant cavity The need for the steering vectors $\mathbf{a}(\omega, \mathbf{r})$ limits the applicability of TR-MUSIC to cases where these vectors are either known analytically or numerically — usually at a high modelling and computational cost. Here, to the best of the authors' knowledge, we present the first application of TR-MUSIC in a resonant cavity. This cavity is used for the localisation of spurious radiation sources in an electromagnetic compatibility pre-compliance test setup. The details of the experiments are presented in [101]. We record on an eight-channel time-reversal mirror the radiation from a short monopole antenna placed at $\mathbf{r}_0$ in a cavity excited by a Gaussian pulse centred at 3 GHz with a 3 GHz bandwidth[8], obtaining the vector $\mathbf{h}(\omega_\ell) = [h_i(\omega_\ell)]_{i=1,\ldots,8}$. The time-reversal matrix is obtained by the outer product $\mathbf{H}(\omega_\ell) = \mathbf{h}^*(\omega_\ell)\mathbf{h}(\omega_\ell)^\top$. From the singular value decomposition of $\mathbf{H}(\omega_\ell)$, we get the left eigenvectors $\mathbf{u}_k(\omega_\ell)$, $k = 1, \ldots, 8$, ordered by decreasing singular values. The steering vectors are obtained experimentally by measuring the scattering parameters between the time-reversal mirror and the short monopole antenna moved on a 100 mm × 100 mm region around the original source location, yielding $\mathbf{a}(\omega_\ell, \mathbf{r}) = [S_{\mathbf{r},i}(\omega_\ell)]_{i=1,\ldots,8}$, where $S_{\mathbf{r},i}(\omega_\ell)$ is the scattering parameter between the time-reversal channel i and the scanner placed at the location $\mathbf{r}$. Finally, the pseudospectrum is computed as

$$P(\mathbf{r}) = \sum_\ell \frac{1}{\sum_{k=2}^{8} |\mathbf{a}^\dagger(\omega_\ell, \mathbf{r})\mathbf{u}_k(\omega_\ell)|} \tag{11}$$

This pseudospectrum, alongside the classical time-reversal result, is shown in Figure 6. As expected, the classical time-reversal approach in Figure 6(a) has a full width at half-maximum of $\sim\lambda_0/1.8$, in agreement with Table 1 for 3D problems (here, λ_0 corresponds to the central frequency of 1.5 GHz). However, the pseudospectrum $P(\mathbf{r})$ displays a full width at half-maximum of $\sim\lambda/19$, displaying super-resolution imaging. This approach could be interesting in electromagnetic compat-

[8] We record 6000 frequency points from 100 kHz to 2.9996 GHz, i.e., every 500 kHz.

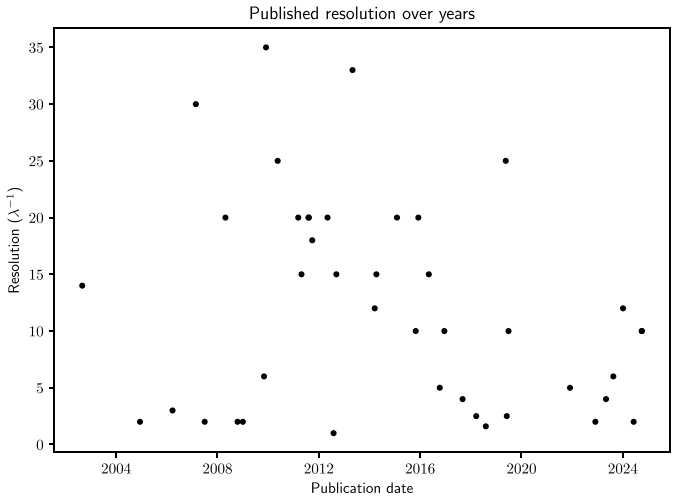

FIGURE 7. Evolution of the achieved super-resolution over time for the references considered in this review.

ibility settings, by leveraging the resolution enhancement of both multiple scattering and MUSIC-based approaches.

3.3.3. Complementary Radar Methods

We briefly summarise methods that do not correspond to DORT or TR-MUSIC alone. Liu et al. investigated [102] radar imaging of reflective target in a cluttered environment, using the difference model with and without targets. Wang et al. [103] combined DORT with TR-MUSIC for a higher computational efficiency, while Engin and Özcan [104] integrated TR-MUSIC with delay estimation MUSIC to image moving targets. An outlying method, which warrants further investigation, is presented by Zhang et al. [105]. The method improves imaging resolution by combining different "looks" (sub-arrays) of an antenna array.

3.3.4. Numerical Methods

There has also been some investigation of super-resolution imaging and focusing in connection with numerical methods. Shi et al. propose [106] an adaptation of the ubiquitous finite-difference, time-domain (FDTD) method for subwavelength structures. Similarly, Wei et al. [107] provide a domain decomposition method to improve FDTD efficiency for subwavelength problems.

In an idiosyncratic set of publications [108–113], So and Hoefer propose to use the transmission-line matrix method with a mesh size that is "too coarse" for the given frequency content to obtain high resolutions in various settings (ergodic cavities, scattering media, non-simultaneous sources). Some further work is needed to measure the impact of the proposed method, notably with respect to the source frequency content and validity with other numerical methods.

3.4. Trends in Resolution

After over twenty years of research into super-resolution in radio-frequency systems, a natural question arises: is there a discernible trend in the achieved resolution? We attempt to answer this question with Figure 7, which illustrates the temporal evolution of reported super-resolution achievements over time. Interestingly, we do not see an increase in the achieved resolution — rather, the opposite seems to hold when analysing the highest resolution over a five-year span. This counter-intuitive trend can be explained by several factors:

1. First, a methodological aspect: once a high resolution has been demonstrated and published with a given method, subsequent studies using the same approach are not expected to re-report the same result.
2. There seem to be several physical constraints limiting, so far, resolutions higher than $\sim\lambda/100$, such as losses, measurement noise, and mismatch between the physical channel and its model (numerical or analytical).
3. Practical applications of super-resolution must also take into account factors other than resolution alone, such as bandwidth, lack of control of the excitation signal, limited field of view, reliability (e.g., a method that yields high resolutions but also requires frequent recalibration might not be attractive for practical applications), high computation burden, etc.
4. Selection bias: some high-resolution methods were excluded because the published images did not allow to derive a full width at half-maximum or minimum source separation — this is especially true in later, more applied work.
5. Finally, in many practical contexts, other performance metrics such as localisation error or signal-to-clutter ratio may be as important as raw resolution.

4. APPLICATIONS OF SUBWAVELENGTH TIME-REVERSAL IMAGING AND FOCUSING

Thanks to its straightforward implementation, time reversal has been adopted in a wide range of applications, which are detailed in this section.

Electromagnetic Compatibility Electromagnetic compatibility (EMC) and antenna performance evaluations are conventionally carried out within anechoic chambers — substantial, high-cost installations designed to eliminate stray reflections. Cozza shows [114] that a modified time-reversal approach can be used in a reverberation chamber to obtain given space- and time-dependences, which could reduce the need for anechoic environments.

Phased-array Diagnostics Maisto et al. use TR-MUSIC to detect faulty elements in a phased-array [115]. A difference model between the reference antenna and a faulty one fed to TR-MUSIC allows detection with reduced data. Compared with compressive sensing, TR-MUSIC requires less prior information.

Resonant Cavities Time-reversal schemes ordinarily exploit the matching of the forward-time propagation channel and its time-reversed backpropagation counterpart — a direct consequence of the reversibility of wave physics. Taddese et al. [116], however, demonstrate that intentional channel mismatches can be equally revealing. By replacing the air in a resonant cavity with gases of differing permittivity (e.g., nitrogen

or helium), they alter the cavity's effective electrical size. A comparison of the chamber's response under standard air conditions versus alternative gas fillings then permits the detection of volume changes as small as 54 parts-per-million.

Wireless Power Transfer Wirelessly powering remote devices is an impactful application where the resolution and frequency band work against each other: lower frequencies reduce cost, complexity, and improve range, but suffer from a diffraction-limited resolution that is usually unacceptable for practical applications. Time reversal has been used to that effect together with a one-dimensional metamaterial to selectively turn on LEDs at a subwavelength scale [117], inside a resonant cavity [118], and numerically explored for selective focusing in concrete [119].

4.1. Radar Imaging

Radar (radio detection and ranging) relies on the echo from reflective targets to an impinging wavefront to form remote images. Practically, an array of antennas use either a multistatic configuration — where transmitters and receivers occupy distinct locations and a multistatic data matrix is built from the transfer functions between each transmit-receive pair — or a monostatic configuration — where emitter and receiver are co-located. The radar time-reversal methods introduced in Section 3.3 (DORT, TR-MUSIC, and their variants) have been applied for moving targets [120, 121], by using average and differential multistatic data matrices [121]. Again, Bahrami et al. observe an increase in resolution in random media [120]. Time reversal has also been used to reduce multipath effects (ghosts in Doppler images) [122]. Finally, Yu et al. propose a low cost experimental setup [123].

Below, we describe a number of specialised applications of radar imaging that have been identified:

Ground-penetrating radar (GPR) This form of radar is developed to locate underground targets, such as buried pipes or landmines [124]. Detecting landmines in conflict zones is crucial for safeguarding civilian populations. Karami et al. propose a review of time-reversal methods for GPR [124] and a detailed performance analysis of TR-MUSIC for landmine detection [125]. Liu et al. [126] combine Green's function for multilayered media to apply TR-MUSIC to subsurface detection.

Through-wall imaging Another flavour of radar consists in locating targets behind a partially reflective object, such as a wall. Zhang et al. [127] use TR-MUSIC with Green's function evaluated with the saddle point method to detect multiple targets through a wall (only numerically in the cited work).

Non-destructive evaluation Defects in composite materials can lead to catastrophic failures. Non-destructive evaluation allows to detect these defects before they become an issue [128]. Mukherjee et al. propose to use time reversal combined with a metamaterial lens [129] to image defects in composites. Finally, Tian et al. show that a combination of DORT and TR-MUSIC is also a viable approach [130].

4.2. Medical Imaging and Focusing

Considerable effort has been devoted to medical imaging and therapeutic focusing — particularly for breast cancer detection and hyperthermia-based tumour treatment. Microwave techniques present several advantages: they are non-ionizing (unlike X-rays) and, in contrast to ultrasound, they probe variations in electrical properties rather than tissue density [131]. Moreover, microwave systems are cost-effective, owing to their relatively simple and inexpensive hardware requirements.

Time-reversal techniques compatible with tomography, such as DORT and TR-MUSIC, have been applied; Hossain et al. [132] also use a combination of beamspace transformation with DORT and TR-MUSIC to improve the signal-to-clutter-ratio in dense fibroglandular tissue clutter. This ratio is more important that resolution alone for the detection of tumours. In a related work, they use a coherent beamspace maximum likelihood method to image highly dense breasts [132]. Given the complexity of data and its acquisition, Fasoula et al. [133] propose a preprocessing scheme that incorporates frequency selection, and spatial filtering modules. Metamaterials, in the form of multi-layered sub-wavelength structures [134] or split-ring embedded square patches [135] have been used to improve imaging. The possibility of using an instantaneous time-reversal mirror (see Section 2.6) to image tumours in heterogeneous, lossy, and dispersive biological media has also been investigated numerically [136]. Casu et al. [137] propose a low-cost off-the-shelf-components-based breast tumour detection setup using a TR-MUSIC related technique known as interferometric MUSIC. Affordable tumour detection methods of this kind are particularly impactful for developing countries.

The dual of imaging, namely focusing, has been used to treat brain tumours via hyperthermia [138] with metasurfaces used for improved focusing. This technique increases the temperature of the cancerous tumour to make it more sensitive to adjunct therapies, such as radiotherapy or chemotherapy.

4.3. Communication

In communication applications, the focusing capability of time-reversal is of particular interest. As discussed in Section 2.2.1, multiple scattering (multipathing) has no detrimental effect on time-reversal focusing: on the contrary, it improves the resolution by enhancing the effective aperture of the time-reversal mirror. Henty and Stancil [139] leverage this phenomenon for communication in an electromagnetically cluttered (work office) environment. They establish two communication channels (instead of one without multiple scattering) between a four-element time-reversal mirror and two subwavelength-spaced locations. Similarly, in random media, Borcea et al. [140] provide estimates of the effective aperture, its link to the focal spot, and a secure communication scheme that leverages propagation randomness. This selective focusing property of time-reversal in complex environments is also used to locate a mmWave user in a "canyon" using Green's function of a multi-layered medium [141], and to mitigate compatibility issues between ultra-wide-band radio devices and IEEE 802.11a systems [142]. Additionally, DORT has been adapted into a multi-frequency variant called cascaded DORT [143] to locate radiated passive

intermodulation sources, a critical challenge for communication systems.

Another approach, mentioned in Section 3.2.4, using microstructured antennas, is used by Ge et al. [144] to selectively communicate with two antennas equipped with complementary split-rings with a subwavelength separation. Without such micro-structuring, a signal encoding a sentence sent simultaneously to both antennas from the time-reversal mirror is not recoverable on the individual antennas. Finally, Wang et al. [145] propose to use time reversal to reduce spurious couplings in a subwavelength MIMO antenna applied to an intra-car communication relay.

5. CONCLUSION

In this review, we have provided a summary of the theoretical foundations of subwavelength time-reversal imaging, covering different aspects such as metrics, multiple scattering, random media, time-reversal cavity, and a seeming contradiction that arises from simplistic conclusions on resolution predictions, time-reversal mirrors, transmission-line networks, instantaneous time-reversal, and the negative transient flux. We saw that methods to obtain super-resolution are based on time-reversal sinks, metamaterials, and algorithms (signal-subspace-based methods and numerical methods). Finally, we surveyed applications of subwavelength imaging and focusing using time reversal in electromagnetic compatibility, phased-array diagnostics, resonant cavities, wireless power transfer, radar imaging, medical imaging and focusing, and radio communications.

To summarize, the recipe of super-resolution imaging and focusing requires three main ingredients: (1) enhancement of the effective aperture of the time-reversal mirror (e.g., through reflections); (2) coupling between the source to image or target to focus at and the time-reversal mirror that enables the propagation of evanescent waves (e.g., through resonance); and (3) postprocessing algorithms that use *a priori* knowledge of the system (e.g., steering vectors in MUSIC-based approaches).

The analysis of the considered references allows us to formulate several methodological recommendations for future work: i) super-resolution claims should always be benchmarked against a diffraction-limited baseline. We note that this baseline is difficult to predict theoretically as highlighted in the varying resolutions reported in Table 1. Likewise, in general, sampling the field at two points at subwavelength distance alone is not enough to ascertain super-resolution. ii) Super-resolution methods that depend on the source characteristics (e.g., location) should, by fairness with other methods, make this limitation explicit and evaluate how resolution varies with different source placements. In a limiting case, one could image sources close to metallic scatterers only, which would artificially enhance the imaging resolution. iii) As imaging problems are a subset of inverse problems, one should be careful to avoid the "inverse crime" [146], i.e., using the same model for both test data acquisition (direct-time stage) and for the backpropagation stage. Doing so can mask issues or artificially enhance the achievable resolution. For instance, drawing on the authors' experience in frequency-domain experimental studies, we first measure the scattering parameter S_{21} coupling the transmitting source (port 1) to the time-reversal mirror (port 2), and then implement time-reversal by backpropagating through the reciprocal channel S_{12}. Committing the inverse crime could consist in using the same physical data, e.g., S_{21} together with an inverse filter, for both forward and reverse propagation. Because both operations share the same noise realisation, the reconstructed image could exhibit spurious super-resolution. By contrast, when the proper cascade is used — $S_{12}S_{21}^{*}$, with independent noise realisations for each step — the image remains constrained by the conventional diffraction limit.

Finally, we highlight some areas that either need further investigation or offer open and new possibilities:

1. The application of the multipole expansion to time reversal is at an early stage. Recent work on the time-domain multipole expansion [147, Figure 3] indicates that the use of high-order multipole moments could be linked with super-resolution. A path towards super-resolution could involve designing metamaterial cells that couple with these higher-order multipole moments.
2. There seems to be no experimental application of active time-reversal sinks for subwavelength imaging or focusing. Also, the issue of negative transient-flux mentioned in Section 3.1 raises the question of whether passive absorbers face inherent performance limits?
3. In general, there is room for exploring links with optimisation or machine-learning techniques to find ways to include prior knowledge into classical time-reversal, akin to the subspace-based methods such as MUSIC.
4. Given that the resolution does not seem to have improved in recent years, could the use of complex frequencies mitigate losses in resonant metalenses, enabling super-resolution better than $\lambda/100$?
5. In electromagnetic compatibility, novel applications of reverberation chambers are of great practical value. How else could signal-subspace methods such as MUSIC be combined with resonant environments?
6. Is there a new paradigm in the work by So and Hoefer on numerical methods? Would it be possible to use data measured or obtained through classical methods, and backpropagate it in an artificial medium that retains the original geometry but allows for subwavelength wave propagation?
7. More generally, mismatch between direct-time experiments and backpropagation, often seen as a limiting factor, was shown to be a powerful imaging tool in Section 4. Could similar time-reversal mismatches enable novel applications such as passive sensing?

APPENDIX A. METHODS

In this appendix, we describe the method used to discover and filter relevant contributions. First, scientific databases were queried for titles, abstracts or keywords containing mentions of time reversal and super-resolution, including syntactic variants. The query used was "(``time revers*'' OR ``time-revers*'') AND (``super resolution'' OR ``super-resolution'' OR ``subwavelength'' OR

``sub-wavelength'' OR ``diffraction limit*'')." The results were next manually filtered by reading all abstracts to determine whether they were relevant to radio frequencies. The result of this process is summarised in Table A1.

TABLE A1. Database results on May 23, 2025. * Results not already present in the Scopus query. † Results not already present in the Scopus and Web of Science queries. ‡ Results not already present in the Scopus, Web of Science, and Google Scholar queries.

Database	Filter	Raw results	Relevant to RF
Scopus	Articles in English	245	78
Web of Science	Articles in English	265	10*
Google Scholar	None	8	0†
IEEE Xplore	All but conference papers	63	14‡

Next, the results were sorted by their number of citations according to Crossref. The result (for the final set of articles) is shown in Figure A1. There is a clear set of five highly-cited, outlying references at more than 150 citations. For all these references, we went through each reference (according to Crossref) and citation (according to Web of Science) to determine whether it needed to be further included in the review. The result from this recursive step is given in Table A2.

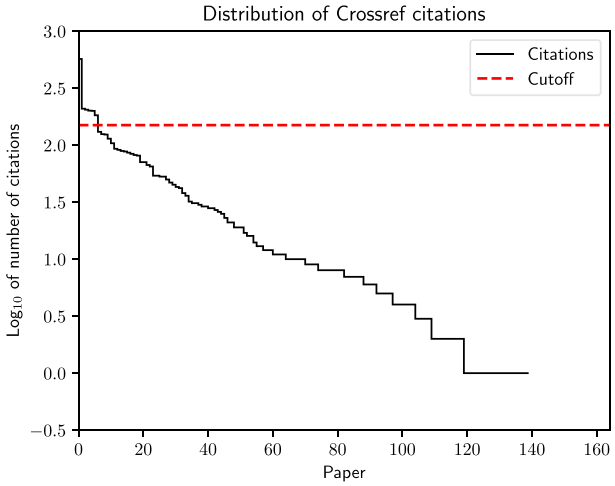

FIGURE A1. Distribution of citations (log scale). Some articles do not have any citation (not shown).

The remaining 132 references were read and classified according to keywords. Of these, some needed to be disqualified. Their number and reason is given in Table A3. During classification and review of the remaining references, ad hoc citations were added when needed. The code and data used to obtain the presented results are publicly available [148].

TABLE A2. Results of the analysis of references and citations of the five most cited references in the initial database results. Results obtained in June 2025. * Additional results not already present in the database.

Item	No. of references	Kept*	No. of citations	Kept*
[71]	22	4	571	9
[45]	5	0	209	6
[58]	25	1	205	1
[94]	13	0	200	12
[49]	14	0	183	2

TABLE A3. Reason for and number of disqualifications from this review. * Theory papers presented in acoustics or optics but that have implications in radio-frequencies were not disqualified.

Reason for disqualification	No. of references
Methodological issues	2
Duplicate entry	1
Not in English	6
Time reversal not involved	17
No imaging or focusing	2
No original research (e.g., review)	10
No super-resolution	9
Not radio-frequencies*	4

REFERENCES

[1] Wang, H., C. J. R. Sheppard, K. Ravi, S. T. Ho, and G. Vienne, "Fighting against diffraction: Apodization and near field diffraction structures," *Laser & Photonics Reviews*, Vol. 6, No. 3, 354–392, May 2012.

[2] Mosk, A. P., A. Lagendijk, G. Lerosey, and M. Fink, "Controlling waves in space and time for imaging and focusing in complex media," *Nature Photonics*, Vol. 6, No. 5, 283–292, May 2012.

[3] Bertolotti, J. and O. Katz, "Imaging in complex media," *Nature Physics*, Vol. 18, No. 9, 1008–1017, Sep. 2022.

[4] Lu, D. and Z. Liu, "Hyperlenses and metalenses for far-field super-resolution imaging," *Nature Communications*, Vol. 3, No. 1, 1205, Nov. 2012.

[5] Glybovski, S. B., S. A. Tretyakov, P. A. Belov, Y. S. Kivshar, and C. R. Simovski, "Metasurfaces: From microwaves to visible," *Physics Reports*, Vol. 634, 1–72, May 2016.

[6] You, J. W., Z. Lan, Q. Ma, Z. Gao, Y. Yang, F. Gao, M. Xiao, and T. J. Cui, "Topological metasurface: From passive toward active and beyond," *Photonics Research*, Vol. 11, No. 3, B65–B102, 2023.

[7] Kumar, A. and W. Arnold, "High resolution in non-destructive testing: A review," *Journal of Applied Physics*, Vol. 132, No. 10, 100901, Sep. 2022.

[8] Ishimaru, A., Y. Kuga, and M. Bright, *Advances in Mathematical Methods for Electromagnetics*, 653–672, IET Digital Library, Dec. 2020.

[9] Wang, Z., S. He, R. Razzaghi, M. Paolone, Y. Xie, and F. Rachidi, "A review of time reversal-based methods applied to fault location in power networks," *Frontiers in Energy Research*, Vol. 10, 1060938, Dec. 2022.

[10] Yavuz, M. E. and F. L. Teixeira, "Ultrawideband microwave sensing and imaging using time-reversal techniques: A review," *Remote Sensing*, Vol. 1, No. 3, 466–495, 2009.

[11] Fink, M., "From Loschmidt daemons to time-reversed waves," *Philosophical Transactions of the Royal Society A: Mathematical, Physical and Engineering Sciences*, Vol. 374, No. 2069, 20150156, Jun. 2016.

[12] Lu, J.-Y., "Reconstruction methods for super-resolution imaging with PSF modulation," *The Journal of the Acoustical Society of America*, Vol. 155, No. 3, A54, Mar. 2024.

[13] Slobozhanyuk, A. P., A. N. Poddubny, A. J. E. Raaijmakers, C. A. T. Van Den Berg, A. V. Kozachenko, I. A. Dubrovina, I. V. Melchakova, Y. S. Kivshar, and P. A. Belov, "Enhancement of magnetic resonance imaging with metasurfaces," *Advanced Materials*, Vol. 28, No. 9, 1832–1838, Mar. 2016.

[14] Brui, E. A., A. V. Shchelokova, M. Zubkov, I. V. Melchakova, S. B. Glybovski, and A. P. Slobozhanyuk, "Adjustable subwavelength metasurface-inspired resonator for magnetic resonance imaging," *Physica Status Solidi (A)*, Vol. 215, No. 5, 1700788, Mar. 2018.

[15] Slobozhanyuk, A. P., I. V. Melchakova, A. V. Kozachenko, D. S. Filonov, C. R. Simovski, and P. A. Belov, "An endoscope based on extremely anisotropic metamaterials for applications in magnetic resonance imaging," *Journal of Communications Technology and Electronics*, Vol. 59, No. 6, 562–570, Jul. 2014.

[16] Gholipour, A., O. Afacan, I. Aganj, B. Scherrer, S. P. Prabhu, M. Sahin, and S. K. Warfield, "Super-resolution reconstruction in frequency, image, and wavelet domains to reduce through-plane partial voluming in MRI," *Medical Physics*, Vol. 42, No. 12, 6919–6932, Dec. 2015.

[17] Gao, K., C. M. Donahue, B. G. Henderson, and R. T. Modrak, "SREMI: Super-resolution electromagnetic imaging with single-channel ground-penetrating radar," *Journal of Applied Geophysics*, Vol. 205, 104777, Oct. 2022.

[18] Astratov, V. N., Y. B. Sahel, Y. C. Eldar, L. Huang, A. Ozcan, N. Zheludev, J. Zhao, Z. Burns, Z. Liu, E. Narimanov, *et al.*, "Roadmap on label-free super-resolution imaging," *Laser & Photonics Reviews*, Vol. 17, No. 12, 2200029, Dec. 2023.

[19] Carminati, R., R. Pierrat, J. de Rosny, and M. Fink, "Theory of the time reversal cavity for electromagnetic fields," *Optics Letters*, Vol. 32, No. 21, 3107–3109, 2007.

[20] Feng, X.-Y., Z. Chen, Z.-M. Xu, and J. Li, "Time-reversal source reconstruction with space and time kurtoses," *IEEE Transactions on Antennas and Propagation*, Vol. 70, No. 6, 4766–4773, Jun. 2022.

[21] Ghaderi Aram, M., M. Haghparast, M. S. Abrishamian, and A. Mirtaheri, "Comparison of imaging quality between linear sampling method and time reversal in microwave imaging problems," *Inverse Problems in Science and Engineering*, Vol. 24, No. 8, 1347–1363, 2016.

[22] Bal, G. and L. Ryzhik, "Time reversal and refocusing in random media," *SIAM Journal on Applied Mathematics*, Vol. 63, No. 5, 1475–1498, 2003.

[23] Fink, M., "Time-reversal waves and super resolution," *Journal of Physics: Conference Series*, Vol. 124, No. 1, 012004, 2008.

[24] Shi, G. and A. Nehorai, "Cramér-Rao bound analysis on multiple scattering in multistatic point-scatterer estimation," *IEEE Transactions on Signal Processing*, Vol. 55, No. 6, 2840–2850, Jun. 2007.

[25] Ammari, H., B. Li, and J. Zou, "Superresolution in recovering embedded electromagnetic sources in high contrast media," *SIAM Journal on Imaging Sciences*, Vol. 13, No. 3, 1467–1510, 2020.

[26] Simonetti, F., "Multiple scattering: The key to unravel the subwavelength world from the far-field pattern of a scattered wave," *Physical Review E*, Vol. 73, No. 3, 036619, Mar. 2006.

[27] Ishimaru, A., S. Jaruwatanadilok, and Y. Kuga, "Imaging through random multiple scattering media using integration of propagation and array signal processing," *Waves in Random and Complex Media*, Vol. 22, No. 1, 24–39, 2012.

[28] Fouque, J. P. and K. Solna, "Time-reversal aperture enhancement," *Multiscale Modeling & Simulation*, Vol. 1, No. 2, 239–259, 2003.

[29] Ishimaru, A., S. Jaruwatanadilok, and Y. Kuga, "Time reversal effects in random scattering media on superresolution, shower curtain effects, and backscattering enhancement," *Radio Science*, Vol. 42, No. 6, 1–9, Dec. 2007.

[30] Chan, T., S. Jaruwatanadilok, Y. Kuga, and A. Ishimaru, "Numerical study of the time-reversal effects on super-resolution in random scattering media and comparison with an analytical model," *Waves in Random and Complex Media*, Vol. 18, No. 4, 627–639, Oct. 2008.

[31] Yavuz, M. E. and F. L. Teixeira, "A numerical study of time-reversed UWB electromagnetic waves in continuous random media," *IEEE Antennas and Wireless Propagation Letters*, Vol. 4, 43–46, 2005.

[32] Gomez, C., "Time-reversal superresolution in random waveguides," *Multiscale Modeling & Simulation*, Vol. 7, No. 3, 1348–1386, 2009.

[33] Papanicolaou, G., K. Solna, and L. Ryzhik, "Statistical stability in time reversal," *SIAM Journal on Applied Mathematics*, Vol. 64, No. 4, 1133–1155, 2004.

[34] Le Boudec, E., N. Mora, F. Rachidi, M. Rubinstein, and F. Vega, "Time-reversed electromagnetic fields in anisotropic media," *Optics Letters*, Vol. 49, No. 7, 1820–1823, 2024.

[35] De Rosny, J. and M. Fink, "Focusing properties of near-field time reversal," *Physical Review A*, Vol. 76, No. 6, 065801, Dec. 2007.

[36] Fannjiang, A. C., "On time reversal mirrors," *Inverse Problems*, Vol. 25, No. 9, 095010, Sep. 2009.

[37] Jaimes, M. A. and R. Snieder, "Spatio-temporal resolution improvement via weighted time-reversal," *Wave Motion*, Vol. 106, 102803, Nov. 2021.

[38] Farhi, A., "Three-dimensional-subwavelength field localization, time reversal of sources, and infinite, asymptotic degeneracy in spherical structures," *Physical Review A*, Vol. 101, No. 6, 063818, Jun. 2020.

[39] Wang, Z., F. Rachidi, M. Paolone, M. Rubinstein, and R. Razzaghi, "A closed time-reversal cavity for electromagnetic waves in transmission line networks," *IEEE Transactions on Antennas and Propagation*, Vol. 69, No. 3, 1621–1630, Mar. 2021.

[40] Wang, Z., R. Razzaghi, M. Paolone, and F. Rachidi, "Electromagnetic time reversal similarity characteristics and its application to locating faults in power networks," *IEEE Transactions on Power Delivery*, Vol. 35, No. 4, 1735–1748, Aug. 2020.

[41] He, S.-Y., A. Cozza, and Y.-Z. Xie, "On the spatial resolution of fault-location techniques based on full-fault transients," *IEEE Transactions on Power Delivery*, Vol. 35, No. 3, 1527–1540, Jun. 2020.

[42] Bal, G., M. Fink, and O. Pinaud, "Time-reversal by time-dependent perturbations," *SIAM Journal on Applied Mathematics*, Vol. 79, No. 3, 754–780, 2019.

[43] Bossy, E. and R. Carminati, "Time-domain radiation and absorption by subwavelength sources," *Europhysics Letters*, Vol. 97, No. 3, 34001, Jan. 2012.

[44] Li, X., P. Li, M.-H. Lu, M. Fink, and G. Ma, "Negative transient flux in the near field of a subwavelength source," *Physical Review Applied*, Vol. 16, No. 1, L011004, Jul. 2021.

[45] De Rosny, J. and M. Fink, "Overcoming the diffraction limit in wave physics using a time-reversal mirror and a novel acoustic sink," *Physical Review Letters*, Vol. 89, No. 12, 124301, Aug. 2002.

[46] Zverev, V. A., "Spatial focusing of a time-reversed pulse," *Radiophysics and Quantum Electronics*, Vol. 46, No. 7, 517–522, Jul. 2003.

[47] Ma, G., X. Fan, F. Ma, J. de Rosny, P. Sheng, and M. Fink, "Towards anti-causal Green's function for three-dimensional sub-diffraction focusing," *Nature Physics*, Vol. 14, No. 6, 608–612, 2018.

[48] Pendry, J. B., "Negative refraction makes a perfect lens," *Physical Review Letters*, Vol. 85, No. 18, 3966, Oct. 2000.

[49] Pendry, J. B., "Time reversal and negative refraction," *Science*, Vol. 322, No. 5898, 71–73, Oct. 2008.

[50] Liao, T.-H., P.-C. Hsieh, and F.-C. Chen, "Subwavelength target detection using ultrawideband time-reversal techniques with a multilayered dielectric slab," *IEEE Antennas and Wireless Propagation Letters*, Vol. 8, 835–838, 2009.

[51] Katko, A. R., G. Shvets, and S. A. Cummer, "Phase conjugation metamaterials: Particle design and imaging experiments," *J. Opt.*, Vol. 14, No. 11, 114003, Jul. 2012.

[52] Grbic, A., L. Jiang, and R. Merlin, "Near-field plates: Subdiffraction focusing with patterned surfaces," *Science*, Vol. 320, No. 5875, 511–513, Apr. 2008.

[53] Goodman, J. W., *Introduction to Fourier Optics*, 2nd ed., 441, McGraw-Hill, New York, 1996.

[54] Le Boudec, E., H. Karami, F. Rachidi, M. Rubinstein, and F. Vega, "Reconciling super-resolution imaging predictions from the time-reversal cavity and Fourier optics," in *2025 URSI AP-RASC*, Sydney, Australia, Aug. 2025.

[55] Massey, G. A., "Microscopy and pattern generation with scanned evanescent waves," *Applied Optics*, Vol. 23, No. 5, 658–660, 1984.

[56] Ellison, W. J., "Permittivity of pure water, at standard atmospheric pressure, over the frequency range 0–25 THz and the temperature range 0–100°C," *Journal of Physical and Chemical Reference Data*, Vol. 36, No. 1, 1–18, Feb. 2007.

[57] Belov, P. A., Y. Hao, and S. Sudhakaran, "Subwavelength microwave imaging using an array of parallel conducting wires as a lens," *Physical Review B*, Vol. 73, No. 3, 033108, Jan. 2006.

[58] Lemoult, F., G. Lerosey, J. de Rosny, and M. Fink, "Resonant metalenses for breaking the diffraction barrier," *Physical Review Letters*, Vol. 104, No. 20, 203901, May 2010.

[59] Lemoult, F., M. Fink, and G. Lerosey, "Revisiting the wire medium: An ideal resonant metalens," *Waves in Random and Complex Media*, Vol. 21, No. 4, 591–613, Oct. 2011.

[60] Belov, P. A., Y. Zhao, S. Tse, P. Ikonen, M. G. Silveirinha, C. R. Simovski, S. Tretyakov, Y. Hao, and C. Parini, "Transmission of images with subwavelength resolution to distances of several wavelengths in the microwave range," *Physical Review B*, Vol. 77, No. 19, 193108, May 2008.

[61] Lemoult, F., M. Fink, and G. Lerosey, "Far-field subwavelength imaging and focusing using a wire medium based resonant metalens," *Waves in Random and Complex Media*, Vol. 21, No. 4, 614–627, 2011.

[62] Guan, F., X. Guo, K. Zeng, S. Zhang, Z. Nie, S. Ma, Q. Dai, J. Pendry, X. Zhang, and S. Zhang, "Overcoming losses in superlenses with synthetic waves of complex frequency," *Science*, Vol. 381, No. 6659, 766–771, Aug. 2023.

[63] Lemoult, F., A. Ourir, J. de Rosny, A. Tourin, M. Fink, and G. Lerosey, "Time reversal in subwavelength-scaled resonant media: Beating the diffraction limit," *International Journal of Microwave Science and Technology*, Vol. 2011, No. 1, 425710, 2011.

[64] Ourir, A., G. Lerosey, F. Lemoult, M. Fink, and J. de Rosny, "Far field subwavelength imaging of magnetic patterns," *Applied Physics Letters*, Vol. 101, No. 11, 111102, Sep. 2012.

[65] Dupré, M., F. Lemoult, M. Fink, and G. Lerosey, "Exploiting spatiotemporal degrees of freedom for far-field subwavelength focusing using time reversal in fractals," *Physical Review B*, Vol. 93, No. 18, 180201, May 2016.

[66] Gong, Z.-S., B.-Z. Wang, Y. Yang, H.-C. Zhou, S. Ding, and X.-H. Wang, "Far-field super-resolution imaging of scatterers with a time-reversal system aided by a grating plate," *IEEE Photonics Journal*, Vol. 9, No. 1, 1–8, Feb. 2017.

[67] Wang, X.-H., M. Hu, B.-Z. Wang, G. Zheng, and P. Chen, "Near-field periodic subwavelength holey metallic plate for far-field superresolution focusing," *IEEE Photonics Journal*, Vol. 9, No. 1, 1–7, Feb. 2017.

[68] Chen, W., L. Deng, K. L. Chung, M. Qu, and B. Feng, "Metasurface-based time-reversal interpolation method for electromagnetic focusing in complex scattering environments," *IEEE Transactions on Antennas and Propagation*, Vol. 72, No. 7, 5782–5793, Jul. 2024.

[69] Wang, R., J. Liu, Y. Lv, Z. Wang, S. Liu, M. Zhang, S. Ding, and B.-Z. Wang, "Subwavelength field shaping approach based on time reversal technique and defective metasurfaces," *IEEE Access*, Vol. 7, 84 629–84 636, 2019.

[70] De Rosny, J., G. Lerosey, and M. Fink, "Theory of electromagnetic time-reversal mirrors," *IEEE Transactions on Antennas and Propagation*, Vol. 58, No. 10, 3139–3149, Oct. 2010.

[71] Lerosey, G., J. de Rosny, A. Tourin, and M. Fink, "Focusing beyond the diffraction limit with far-field time reversal," *Science*, Vol. 315, No. 5815, 1120–1122, Feb. 2007.

[72] Ge, G.-D., R. Zang, D. Wang, S. Ding, and B.-Z. Wang, "Subwavelength array of planar antennas with defect oval rings based on far-field time reversal," *Electronics Letters*, Vol. 47, No. 16, 901–903, Aug. 2011.

[73] Ge, G.-D., D. Wang, and B.-Z. Wang, "Subwavelength array of planar triangle monopoles with cross slots based on far-field time reversal," *Progress In Electromagnetics Research*, Vol. 114, 429–441, 2011.

[74] Liang, M.-S. and B.-Z. Wang, "A miniaturized subwavelength array of planar monopoles based on far-field time reversal," in *2012 International Conference on Microwave and Millimeter Wave Technology (ICMMT)*, 1–4, Shenzhen, China, May 2012.

[75] Ding, S., B.-Z. Wang, G. Ge, and D. Zhao, "Sub-wavelength array with embedded chirped delay lines based on time reversal technique," *IEEE Transactions on Antennas and Propagation*, Vol. 61, No. 5, 2868–2873, May 2013.

[76] Huang, H.-Y., S. Ding, B.-Z. Wang, and R. Zang, "Split-ring-based metamaterial for far-field subwavelength focusing based on time reversal," *Chinese Physics B*, Vol. 23, No. 6, 064101, 2014.

[77] Yang, C., M. Zhu, C. Zhou, and D. Zhao, "Sub-wavelength UWB antenna array with fractal slots and split ring resonators for time reversal super-resolution focusing," in *2014 IEEE International Conference on Communiction Problem-Solving*, 173–175, Beijing, China, Dec. 2014.

[78] Gao, Q., B.-Z. Wang, and X.-H. Wang, "Far-field super-resolution imaging with compact and multifrequency planar resonant lens based on time reversal," *IEEE Transactions on Antennas and Propagation*, Vol. 63, No. 12, 5586–5592, Dec. 2015.

[79] Ding, S., S. Gupta, R. Zang, L. Zou, B.-Z. Wang, and C. Caloz, "Enhancement of time-reversal subwavelength wireless transmission using pulse shaping," *IEEE Transactions on Antennas and Propagation*, Vol. 63, No. 9, 4169–4174, Sep. 2015.

[80] Liang, M.-S., B.-Z. Wang, Z.-M. Zhang, and S. Ding, "Simplified pulse shaping network for microwave signal focusing based on time reversal," *IEEE Antennas and Wireless Propagation Letters*, Vol. 14, 225–228, 2015.

[81] Wang, R., B.-Z. Wang, Y. Yang, M.-S. Liang, Z.-S. Gong, and X. Ding, "Compact multiport antenna for time reversal communication system," in *2015 Asia-Pacific Microwave Conference (APMC)*, 1–3, Nanjing, China, Dec. 2015.

[82] Tu, H., S. Xiao, D. Lesselier, and M. Serhir, "Super-resolution characteristics based on time-reversed single-frequency electromagnetic wave," *Journal of Electromagnetic Waves and Applications*, Vol. 30, No. 13, 1670–1680, 2016.

[83] Tu, H.-L. and S.-Q. Xiao, "Investigation of the effects of metal-wire resonators in sub-wavelength array based on time-reversal technique," *AIP Advances*, Vol. 6, No. 5, 055001, May 2016.

[84] Wang, K., W. Shao, H. Ou, and B.-Z. Wang, "Time-reversal focusing beyond the diffraction limit using near-field auxiliary sources," *IEEE Antennas and Wireless Propagation Letters*, Vol. 16, 2828–2831, 2017.

[85] Yang, X.-S., M.-M. Zhang, T. Li, and B.-Z. Wang, "A compact MIMO antenna and its time reversal super-resolution focusing," in *2018 IEEE Asia-Pacific Conference on Antennas and Propagation (APCAP)*, 118–119, Auckland, New Zealand, Aug. 2018.

[86] Twumasi, B. A. and J.-L. Li, "Numerical simulation study on bowtie antenna-based time reversal mirror for super-resolution target detection," *Journal of Electrical Engineering*, Vol. 70, No. 3, 236–243, Jun. 2019.

[87] Gao, Q. and X.-Q. Li, "Wideband far-field super-resolution focusing based on composite metalens," in *2019 International Conference on Microwave and Millimeter Wave Technology (ICMMT)*, 1–3, Guangzhou, China, May 2019.

[88] Ran, P., S. Chen, M. Serhir, and D. Lesselier, "Imaging of sub-wavelength microstructures by time reversal and neural networks, from synthetic to laboratory-controlled data," *IEEE Transactions on Antennas and Propagation*, Vol. 69, No. 12, 8753–8762, Dec. 2021.

[89] Ricker, N., "Wavelet functions and their polynomials," *Geophysics*, Vol. 9, No. 3, 287–409, Jul. 1944.

[90] Prada, C., S. Manneville, D. Spoliansky, and M. Fink, "Decomposition of the time reversal operator: Detection and selective focusing on two scatterers," *The Journal of the Acoustical Society of America*, Vol. 99, No. 4, 2067–2076, Apr. 1996.

[91] Gao, W., X.-H. Wang, and B.-Z. Wang, "Time-reversal ESPRIT imaging method for the detection of single target," *Journal of Electromagnetic Waves and Applications*, Vol. 28, No. 5, 634–640, 2014.

[92] Schmidt, R., "Multiple emitter location and signal parameter estimation," *IEEE Transactions on Antennas and Propagation*, Vol. 34, No. 3, 276–280, Mar. 1986.

[93] Lehman, S. K. and A. J. Devaney, "Transmission mode time-reversal super-resolution imaging," *The Journal of the Acoustical Society of America*, Vol. 113, No. 5, 2742–2753, May 2003.

[94] Devaney, A. J., "Time reversal imaging of obscured targets from multistatic data," *IEEE Transactions on Antennas and Propagation*, Vol. 53, No. 5, 1600–1610, May 2005.

[95] Davy, M., J.-G. Minonzio, J. de Rosny, C. Prada, and M. Fink, "Influence of noise on subwavelength imaging of two close scatterers using time reversal method: Theory and experiments," *Progress In Electromagnetics Research*, Vol. 98, 333–358, 2009.

[96] Solimene, R. and A. Dell'Aversano, "Some remarks on time-reversal MUSIC for two-dimensional thin PEC scatterers," *IEEE Geoscience and Remote Sensing Letters*, Vol. 11, No. 6, 1163–1167, Jun. 2014.

[97] Cheng, Z.-H., H. Li, C. Huang, D. Zhao, and B.-Z. Wang, "Tradeoff of computational complexity and accuracy in space frequency time reversal imaging," *IEEE Sensors Journal*, Vol. 25, No. 3, 4980–4989, 2025.

[98] Choi, H., Y. Ogawa, T. Nishimura, and T. Ohgane, "Time-reversal MUSIC imaging with time-domain gating technique," *IEICE Transactions on Communications*, Vol. E95-B, No. 7, 2377–2385, 2012.

[99] Moura, J. M. F. and Y. Jin, "Time reversal imaging by adaptive interference canceling," *IEEE Transactions on Signal Processing*, Vol. 56, No. 1, 233–247, Jan. 2008.

[100] Solimene, R., A. Dell'Aversano, and G. Leone, "Interferometric time reversal MUSIC for small scatterer localization," *Progress In Electromagnetics Research*, Vol. 131, 243–258, 2012.

[101] Le Boudec, E., H. Karami, D. Martinez, F. Rachidi, M. Rubinstein, and F. Vega, "Single-shot experimental localization of electromagnetic interference sources with application to electrostatic discharges," *URSI Radio Science Letters*, Vol. 7, 2025.

[102] Liu, D., G. Kang, L. Li, Y. Chen, S. Vasudevan, W. Joines, Q. H. Liu, J. Krolik, and L. Carin, "Electromagnetic time-reversal imaging of a target in a cluttered environment," *IEEE Transactions on Antennas and Propagation*, Vol. 53, No. 9, 3058–3066, Sep. 2005.

[103] Wang, X., W. Gao, and B. Wang, "Efficient hybrid method for time reversal superresolution imaging," *Journal of Systems Engineering and Electronics*, Vol. 26, No. 1, 32–37, Feb. 2015.

[104] Engin, E. and M. Özcan, "Moving target detection using super-resolution algorithms with an ultra wideband radar," *International Journal of Imaging Systems and Technology*, Vol. 20, No. 3, 237–244, 2010.

[105] Zhang, G., J. Zhu, J. Li, and N. Wang, "High-resolution imaging algorithm based on temporal focal characteristic of time-reversed signal," *Systems Science & Control Engineering*, Vol. 7, No. 1, 198–209, 2019.

[106] Shi, S.-B., W. Shao, J. Ma, C. Jin, and X.-H. Wang, "Newmark-Beta-FDTD method for super-resolution analysis of time reversal waves," *Journal of Computational Physics*, Vol. 345, 475–483, Sep. 2017.

[107] Wei, X.-K., W. Shao, H. Ou, and B.-Z. Wang, "Efficient WLP-FDTD with complex frequency-shifted PML for super-resolution analysis," *IEEE Antennas and Wireless Propagation Letters*, Vol. 16, 1007–1010, 2017.

[108] So, P. P. M. and W. J. R. Hoefer, "A new look at computational time reversal in TLM," in *2014 International Conference on Numerical Electromagnetic Modeling and Optimization for RF, Microwave, and Terahertz Applications (NEMO)*, 1–4, Pavia, Italy, May 2014.

[109] So, P. P. M. and W. J. R. Hoefer, "Source reconstruction with superresolution using TLM time reversal," in *2014 IEEE MTT-S International Microwave Symposium (IMS2014)*, 1–4, Tampa, FL, USA, Jun. 2014.

[110] Hoefer, W. J. R. and P. P. M. So, "Reconstruction of non-simultaneous impulsive sources with superresolution in TLM by computational time reversal," in *2015 IEEE MTT-S International Microwave Symposium*, 1–3, Phoenix, AZ, USA, May 2015.

[111] Hoefer, W. J. R., "Superresolution imaging by computational time reversal in scattering media," in *2015 IEEE International Symposium on Antennas and Propagation & USNC/URSI National Radio Science Meeting*, 1302–1303, Vancouver, BC, Canada, Jul. 2015.

[112] Hoefer, W. J. R., "Computational time reversal — A frontier in electromagnetic structure synthesis and design," *IEEE Transactions on Microwave Theory and Techniques*, Vol. 63, No. 1, 3–10, Jan. 2015.

[113] Hoefer, W. J. R. and P. P. M. So, "A scattering slab and time reversal make a computational superlens," in *2015 IEEE MTT-S International Conference on Numerical Electromagnetic and Multiphysics Modeling and Optimization (NEMO)*, 1–3, Ottawa, ON, Canada, Aug. 2015.

[114] Cozza, A., "Emulating an anechoic environment in a wave-diffusive medium through an extended time-reversal approach," *IEEE Transactions on Antennas and Propagation*, Vol. 60, No. 8, 3838–3852, Aug. 2012.

[115] Maisto, M. A., M. D. Prete, A. Cuccaro, and R. Solimene, "Near-field phased array diagnostics by a subspace projection method," *IEEE Access*, Vol. 12, 80 283–80 299, 2024.

[116] Taddese, B. T., G. Gradoni, F. Moglie, T. M. Antonsen, E. Ott, and S. M. Anlage, "Quantifying volume changing perturbations in a wave chaotic system," *New Journal of Physics*, Vol. 15, No. 2, 023025, Feb. 2013.

[117] Chabalko, M. J. and A. P. Sample, "Electromagnetic time reversal focusing of near field waves in metamaterials," *Applied Physics Letters*, Vol. 109, No. 26, 263901, Dec. 2016.

[118] Cheng, Z.-H., T. Li, L. Hu, X. Ma, F. Liang, D. Zhao, and B.-Z. Wang, "Selectively powering multiple small-size devices spaced at diffraction limited distance with point-focused electromagnetic waves," *IEEE Transactions on Industrial Electronics*, Vol. 69, No. 12, 13 696–13 705, Dec. 2022.

[119] Twumasi, B. A., J.-L. Li, F. K. Deynu, E. T. Ashong, C. Dzah, and D. Pomary, "Selective microwave wireless power transfer to sensors embeddedin concrete at sub-wavelength spacing using electromagnetictime-reversal technique," *Applied Computational Electromagnetics Society Journal (ACES)*, Vol. 39, No. 4, 364–375, Apr. 2024.

[120] Bahrami, S., A. Cheldavi, and A. Abdolali, "Moving target tracking using time reversal method," *Progress In Electromagnetics Research M*, Vol. 25, 39–52, 2012.

[121] Fouda, A. E. and F. L. Teixeira, "Imaging and tracking of targets in clutter using differential time-reversal techniques," *Waves in Random and Complex Media*, Vol. 22, No. 1, 66–108, 2012.

[122] De Arriba-Ruiz, I., J. M. Muñoz-Ferreras, and F. Pérez-Martínez, "Multipath mitigation techniques based on time reversal concept and superresolution algorithms for inverse synthetic aperture radar imaging," *IET Radar, Sonar & Navigation*, Vol. 7, No. 4, 413–421, 2013.

[123] Yu, Z., J. Pan, D. Yang, and X. Xie, "Time-divided multichannel technique for EM-TRM based object detection system in complex environment," in *2009 Asia Pacific Microwave Conference*, 2328–2331, Singapore, Dec. 2009.

[124] Karami, H., A. Koch, C. Romero, M. Rubinstein, and F. Rachidi, "Landmine detection using electromagnetic time reversalbased methods: 1. Classical TR, iterative TR, DORT and TR-MUSIC," *Radio Science*, Vol. 59, No. 10, 1–13, 2024.

[125] Karami, H., A. Koch, C. Romero, M. Rubinstein, and F. Rachidi, "Landmine detection using electromagnetic time reversal-based methods: 2. Performance analysis of TR-MUSIC," *Radio Science*, Vol. 59, No. 10, e2024RS007972, 2024.

[126] Liu, X.-F., B.-Z. Wang, and S.-Q. Xiao, "Electromagnetic subsurface detection using subspace signal processing and half-space dyadic Green's function," *Progress In Electromagnetics Research*, Vol. 98, 315–331, 2009.

[127] Zhang, W., A. Hoorfar, and L. Li, "Through-the-wall target localization with time reversal MUSIC method," *Progress In Electromagnetics Research*, Vol. 106, 75–89, 2010.

[128] Mukherjee, S., Z. Su, L. Udpa, S. Udpa, and A. Tamburrino, "Enhancement of microwave imaging using a metamaterial lens," *IEEE Sensors Journal*, Vol. 19, No. 13, 4962–4971, Jul. 2019.

[129] Mukherjee, S., X. Shi, S. Datta, Y. Deng, S. Udpa, and L. Udpa, "Enhancement of microwave time reversal imaging using metallic reflectors," *NDT & E International*, Vol. 110, 102192, Mar. 2020.

[130] Tian, S., X. Yang, H. Peng, T. Zhang, F. Gao, and J. Wu, "Frequency domain time reversal adaptive focusing on nondestructive testing imaging method for composite materials," *Journal of Nondestructive Evaluation*, Vol. 44, No. 3, 82, 2025.

[131] Hossain, M. D., A. S. Mohan, and M. J. Abedin, "Beamspace time-reversal microwave imaging for breast cancer detection," *IEEE Antennas and Wireless Propagation Letters*, Vol. 12, 241–244, 2013.

[132] Hossain, M. D. and A. S. Mohan, "Cancer detection in highly dense breasts using coherently focused time-reversal microwave imaging," *IEEE Transactions on Computational Imaging*, Vol. 3, No. 4, 928–939, Dec. 2017.

[133] Fasoula, A., B. M. Moloney, L. Duchesne, J. D. G. Cano, B. L. Oliveira, J.-G. Bernard, and M. J. Kerin, "Super-resolution radar imaging for breast cancer detection with microwaves: The integrated information selection criteria," in *2019 41st Annual International Conference of the IEEE Engineering in Medicine and Biology Society (EMBC)*, 1868–1874, Berlin, Germany, Jul. 2019.

[134] Twumasi, B. A., J.-L. Li, and C. Dzah, "Sensitivity enhancement of super resolution breast tumour imaging with far-field time reversal mirror integrating with multi-layered sub-wavelength patch scatterers," *Journal of Physics D: Applied Physics*, Vol. 53, No. 7, 075401, Dec. 2019.

[135] Twumasi, B. A., J.-L. Li, E. T. Ashong, C. Dzah, and D. Pomary, "Time reversal mirror for hyperthermia of multi-focal breast tumors using electromagnetic time reversal technique," *Electromagnetics*, Vol. 42, No. 8, 594–615, 2022.

[136] Wu, C. T., N. M. Nobre, E. Fort, G. D. Riley, and F. Costen, "Tailoring instantaneous time mirrors for time reversal focusing in absorbing media," *IEEE Transactions on Antennas and Propagation*, Vol. 70, No. 10, 9630–9640, Oct. 2022.

[137] Casu, M. R., M. Vacca, J. A. Tobon, A. Pulimeno, I. Sarwar, R. Solimene, and F. Vipiana, "A COTS-based microwave imaging system for breast-cancer detection," *IEEE Transactions on Biomedical Circuits and Systems*, Vol. 11, No. 4, 804–814, Aug. 2017.

[138] Hajiahmadi, M. J., R. Faraji-Dana, and C. Caloz, "Metasurface-based time-reversal focusing for brain tumor microwave hyperthermia," *IEEE Transactions on Antennas and Propagation*, Vol. 70, No. 12, 12 237–12 246, Dec. 2022.

[139] Henty, B. E. and D. D. Stancil, "Multipath-enabled super-resolution for RF and microwave communication using phase-conjugate arrays," *Physical Review Letters*, Vol. 93, No. 24, 243904, Dec. 2004.

[140] Borcea, L., G. Papanicolaou, and C. Tsogka, "Theory and applications of time reversal and interferometric imaging," *Inverse Problems*, Vol. 19, No. 6, S139, Nov. 2003.

[141] Zakeri, M. J. and S. Sadeghi, "Electromagnetic time-reversal positioning of a single user in a street canyon scenario," *Journal of Electromagnetic Waves and Applications*, Vol. 39, No. 13, 1600–1618, Jun. 2025.

[142] Liu, J., D. Zhao, B.-Z. Wang, J. Dou, and G. Ge, "Time-reversal method for coexistence between ultrawideband radios and IEEE802.11a systems," *IEEE Transactions on Electromagnetic Compatibility*, Vol. 53, No. 4, 1065–1071, Nov. 2011.

[143] Guo, Z., Z. Cheng, L. Chen, and D. Zhao, "Resolution-enhanced and accurate cascade time-reversal operator decomposition (C-DORT) approach for positioning radiated passive intermodulation sources," *Electronics*, Vol. 12, No. 9, 2104, 2023.

[144] Ge, G.-D., B.-Z. Wang, D. Wang, D. Zhao, and S. Ding, "Subwavelength array of planar monopoles with complementary split rings based on far-field time reversal," *IEEE Transactions on Antennas and Propagation*, Vol. 59, No. 11, 4345–4350, Nov. 2011.

[145] Wang, R., B.-Z. Wang, Z.-S. Gong, and X. Ding, "Compact multiport antenna with radiator-sharing approach and its performance evaluation of time reversal in an intra-car environment," *IEEE Transactions on Antennas and Propagation*, Vol. 63, No. 9, 4213–4219, Sep. 2015.

[146] Colton, D. and R. Kress, *Inverse Acoustic and Electromagnetic Scattering Theory*, Springer, Cham, Switzerland, 2019.

[147] Le Boudec, E., C. Kasmi, N. Mora, F. Rachidi, E. Radici, M. Rubinstein, and F. Vega, "The time-domain Cartesian multipole expansion of electromagnetic fields," *Scientific Reports*, Vol. 14, No. 1, 8084, Apr. 2024.

[148] Le Boudec, E., Eliasleb/Subwavelength_emtr_review: Zenodov2 version v2, Zenodo, https://doi.org/10.5281/zenodo.15944905, Jul. 2025.